

## Article

# Insights into the Metallogenesis of the Felsic Volcanic Hosted Mundiyawas-Khera Cu Deposit, Alwar Basin, Western India

Janmejaya Sahoo <sup>1,2</sup>, Prabodha Ranjan Sahoo <sup>1,\*</sup>, Israel Khan <sup>1,3</sup> and Akella Satya Venkatesh <sup>1</sup>

<sup>1</sup> Department of Applied Geology, Indian Institute of Technology (Indian School of Mines), Dhanbad 826004, India; jsjanmejaya@gmail.com (J.S.); israilkhangsi786@gmail.com (I.K.); asvenkatesh@iitism.ac.in (A.S.V.)

<sup>2</sup> Geological Survey of India, Hyderabad 500068, India

<sup>3</sup> Geological Survey of India, Bhubaneswar 751012, India

\* Correspondence: prabodha@iitism.ac.in; Tel.: +91-326-2235112

**Abstract:** Copper and associated gold mineralization in the Mundiyawas-Khera area of western India is hosted by the Proterozoic felsic volcanic rocks of rhyo-dacite composition. Signatures of hydrothermal alteration represented by sericite, epidote, scapolite and carbonates are well observed around the ore mineralization zone. The felsic volcanic rocks with gently to flat sloping REE pattern, variable negative Eu anomaly, intermediate abundances of HFSE and moderate to low Zr/Y anomalies are suggested to be FII, FIIIa and FIV type rhyolite. The felsic volcanic host rock for copper mineralization has a depleted and flat HREE pattern and indicates the crustal source, which is garnet free. Negative Eu anomaly in the rock is probably because of the intracrustal partial melting formed in a rift related environment. The high temperature magmatic activities are probably evolved due to the partial melting of crust at shallow to moderate depths, suggesting an evolved continental crust. The  $\delta^{13}\text{C}$  values of the mineralized carbonate veins range between  $-10.4\text{\textperthousand}$  and  $-0.9\text{\textperthousand}$  (min =  $-10.6\text{\textperthousand}$ ,  $n = 27$ ), whereas the  $\delta^{18}\text{O}$  values show a range of  $16.35\text{\textperthousand}$  to  $25.23\text{\textperthousand}$  (min =  $21.49\text{\textperthousand}$ ,  $n = 27$ ), ideally suggesting a mixed source for the ore bearing fluid. Geological, geochemical and stable isotope data of the Mundiyawas-Khera copper deposit suggest it to be a VMS/VHMS setup and these insights will lead to finding new deposits in the nearby areas, having same stratigraphic horizons and similar lithogeochemical assemblages.



**Citation:** Sahoo, J.; Sahoo, P.R.; Khan, I.; Venkatesh, A.S. Insights into the Metallogenesis of the Felsic Volcanic Hosted Mundiyawas-Khera Cu Deposit, Alwar Basin, Western India. *Minerals* **2022**, *12*, 370. <https://doi.org/10.3390/min12030370>

Academic Editors: Aida Maria Conte, Cristina Perinelli, Michela Ingrassia and Liqiang Yang

Received: 25 January 2022

Accepted: 11 March 2022

Published: 17 March 2022

**Publisher's Note:** MDPI stays neutral with regard to jurisdictional claims in published maps and institutional affiliations.



**Copyright:** © 2022 by the authors. Licensee MDPI, Basel, Switzerland. This article is an open access article distributed under the terms and conditions of the Creative Commons Attribution (CC BY) license (<https://creativecommons.org/licenses/by/4.0/>).

## 1. Introduction

Copper mineralization mainly occurs in a wide variety of geologic environments among which the magmatic copper sulfides, porphyry copper deposits, iron oxide copper-gold (IOCG), volcanogenic massive sulfide (VMS) or volcanic-hosted massive sulfide (VHMS) and sediment-hosted copper deposits are very significant [1–3]. Different copper deposit types are characterized by their litho-association, ore mineralogy, fluid characteristics, alteration patterns and stable isotopic signatures [4,5]. The VMS/VHMS deposits occur in a wide variety of geologic environments and throughout geologic history, starting from the Archean (e.g., deposits in the Slave and Abitibi-Superior provinces in Canada [6]) to the modern day (e.g., the Solwara-1 and Solwara-2 deposits in deep seawater in Papua New Guinea [3]). They are distributed worldwide and range in size varying from insignificant to giant, with world-class deposits such as Kidd Creek, Ontario and Windy Craggy, British Columbia [3]. The origin of the deposit can be well understood through host rock geochemistry, alteration patterns, ore mineral associations and isotopic signatures and has wide application in mineral exploration. Distinct hydrothermal alteration patterns are observed both in the porphyry and VMS setting [7,8]. The alteration patterns are the gross effect of the interaction between the metal bearing hydrothermal fluid and the country

rocks. Hence, host rock lithogeochemistry and mineral association can be the tracers for types of copper deposit.

In western India, the Proterozoic Aravalli Delhi Fold Belt (ADFB) hosts a number of world class base metal deposits, e.g., Pb-Zn deposits of Agucha, Rajpura-Dariba, Zawar and Khetri copper belt [9–12]. These base metal deposits are controlled both by the lithology and the structural geometry of the terrain. Apart from these, smaller occurrences of low to medium grade copper mineralization are found in the Nim ka Thana and Alwar basin [13–15]. The present study is focused on the Mundiyawas-Khera copper-gold deposits located in Alwar basin [13,14]. This deposit was discovered by Geological Survey of India (GSI) through different stages of exploration [13,14,16]. Detailed exploration and preliminary geochemical characterization of the ore and host rocks have been conducted by GSI [13,14,16–18]. Geophysical and remote sensing study of the area have also been carried out to understand the spatial distribution of the ore body and alteration patterns respectively [19,20]. However, detailed geochemical study of ore and host rocks, source of ore bearing fluids, alterations and classification of the deposit have not yet been effectively attempted. The ore forming processes of the study area are unclear and need detailed investigation. Unlike the well-established copper deposit in Khetri, which has been classified as an IOCG type deposit [11,12], the Mundiyawas-Khera copper deposit is relatively smaller with an average grade of 0.41% with distinct variation in the lithological assemblages as well as nature of mineralization and alteration phenomena. As per the present understanding, stratigraphically, this is also hosted within a younger volcano-sedimentary sequence [14]. This paper deals with the lithogeochemistry, petrography and wall rock alteration coupled with stable isotope (Carbon and Oxygen isotopes) studies of the copper mineralizing system to constrain the conditions for the metallogenesis of the Mundiyawas-Khera copper deposit. This will be a major implication for strategic exploration planning and refinement of metallogenetic model vector to explore new deposits in nearby areas.

## 2. Geological Setting

### 2.1. Regional Geology

The NNE-SSW trending Aravalli and Delhi Fold Belts are located in the western part of the Indian peninsula (Figure 1). They are the treasure of some classic polymetallic sulfide deposits [9–15,21]. The vast expanse of gneiss–migmatite–amphibolitic rocks, generally referred to as Banded Gneissic Complex (BGC), is characterized as the basement of these belts [22]. The basement complex has experienced granitoid magmatism from 1.73 to 1.72 Ga and by metamorphic events during 1.85 Ga, 1.73 Ga, 1.62 Ga and 1.0–0.95 Ga [23–28]. The two supracrustal units, namely the Palaeoproterozoic Aravalli fold belt (AFB) and the Meso-Neo Proterozoic Delhi fold belt (DFB), are overlain on Achaean basement and are known as Aravalli Supergroup and Delhi Supergroup respectively [22,29–32]. These two-fold belts are presumed to have been formed in a rifted cratonic segment [33–36] with some exhumed oceanic slices/terrains incorporated during the subduction related processes [37,38].

The volcano-sedimentary successions of the Delhi Supergroup are subdivided into North Delhi Fold Belt (NDFB) and South Delhi Fold Belt (SDFB) according to the geographic location, age and degree of metamorphism. The meta-volcano sedimentary units of NDFB are distributed over Lalsot–Bayana, Alwar and Khetri basin (Figure 2) [39–41]. Stratigraphically, the belt is divided into the older Raialo Group (carbonate-dominant), the intermediate Alwar Group (arenaceous-rich) and the younger Ajabgarh Group (argillaceous-rich) [39,41,42]. The meta-volcano sedimentary rocks of the Delhi Supergroup record multiple phases of deformation [43,44] and medium-grade metamorphism at ca. 550 °C and 300–400 MPa [9,41,45–47]. The economic copper mineralization occurs in the Alwar and the Ajabgarh Group of rocks at Khetri, which is classified as an iron oxide–copper–gold (IOCG)-type deposit [11,48,49].

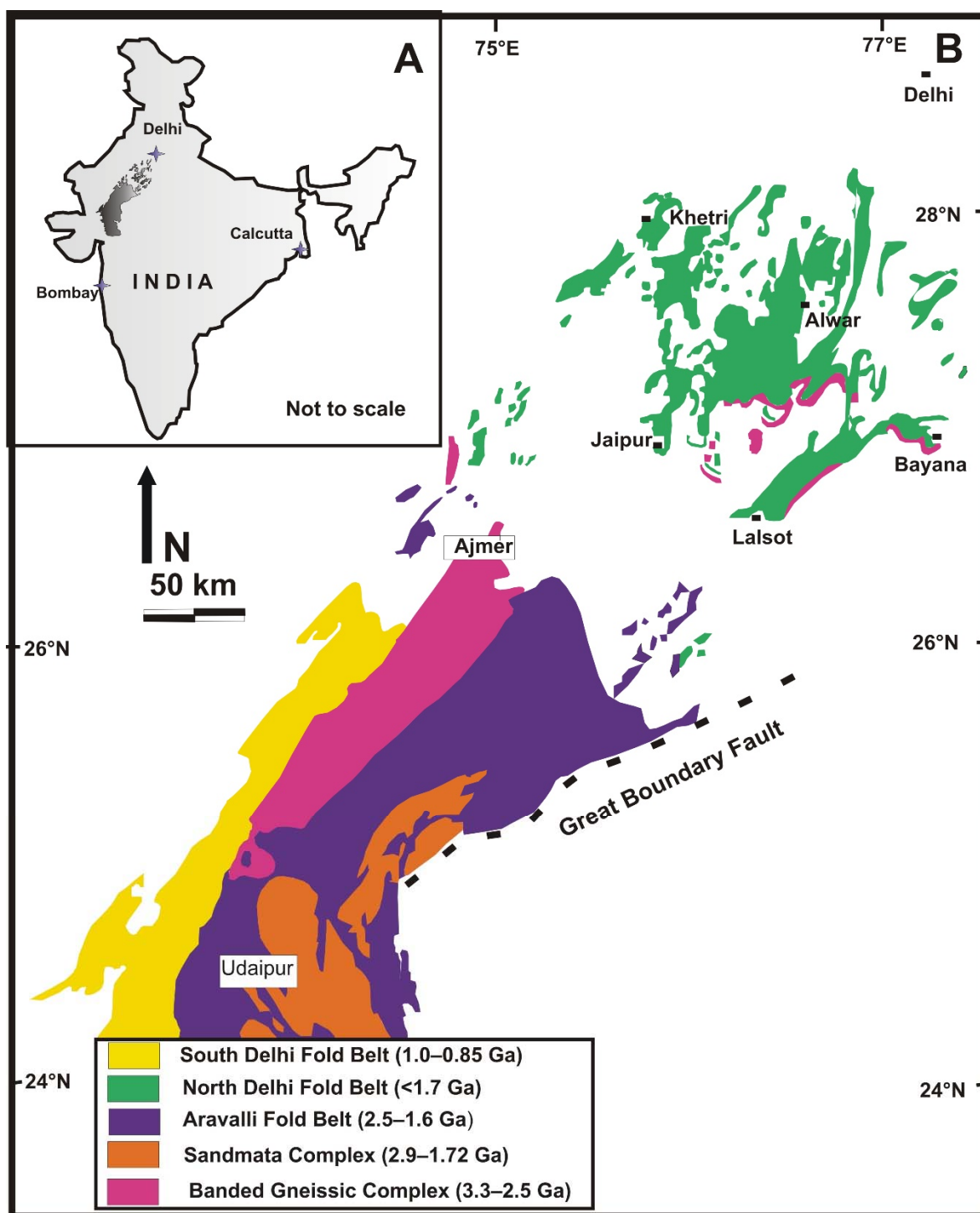


**Figure 1.** (A) Location of Delhi Fold Belt in India map; (B) Generalized regional geological map of the Delhi Fold Belt (modified from [28]).

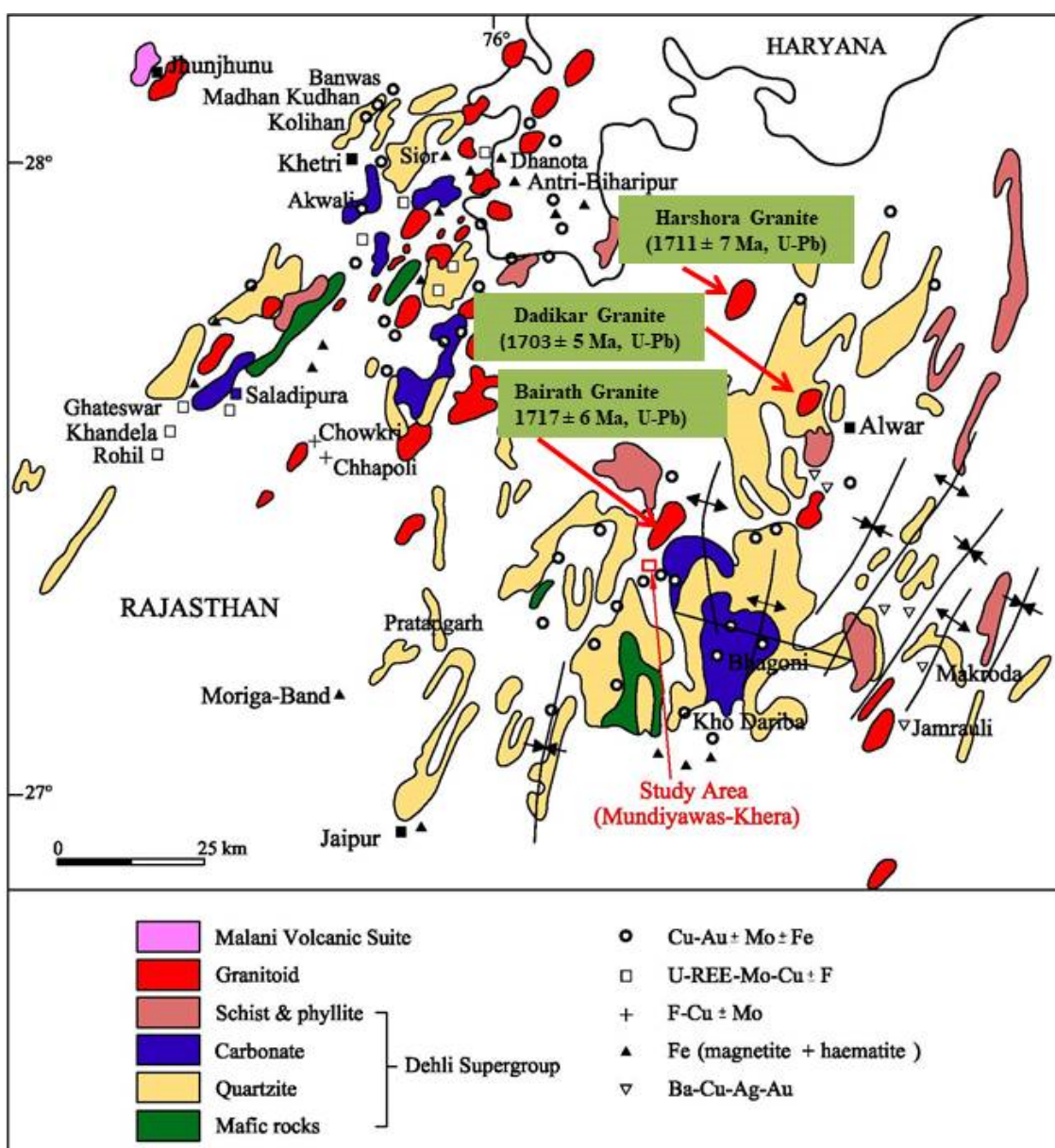


**Figure 2.** Regional geological map of northern Rajasthan and Haryana showing the disposition of Khetri copper belt (KCB) and Kho-Dariba deposit (modified after [11]). The ages of Harshora Granite, Dadikar Granite and Bairath granite are zircon U–Pb age [28].

## 2.2. Deposit Scale Geology

The Mundiyawas-Khera copper deposit is located in the Alwar basin which represents the rock types of Thanagazi Formation of the Ajabgarh Group [14]. The litho types exposed in the study area are the felsic tuffs of rhyo-dacite composition, interlayered with sedimentary sequences composed of quartzite, carbon phyllite and dolomitic marble (Figure 3) [13]. The felsic volcanic rocks are the dominant host for base metal mineralization as established from the surface signatures and borehole sections (Figure 4). Chalcopyrite, pyrrhotite and arsenopyrite are the dominant sulfide minerals observed in the area. Green-schist to lower amphibolite facies of metamorphism is noticed [50] from the mineral assemblages. Four mineralized zones extending for about 400 m along strike with 10–30 m average width of individual zones have been confirmed from the exploration data [17]. Sulfide mineralization is observed in the form of disseminations, stringers, vein lets and fracture filling and locally occur as massive chalcopyrite, arsenopyrite and pyrrhotite (Figure 5). The total

mineral resources of UNFC (332) category estimated for Cu, Au and Ag are 40.49 Mt@ 0.37% Cu, 4.19 Mt@ 0.80 g/t Au and 2.71 Mt@ 7.07 g/t Ag respectively [18].

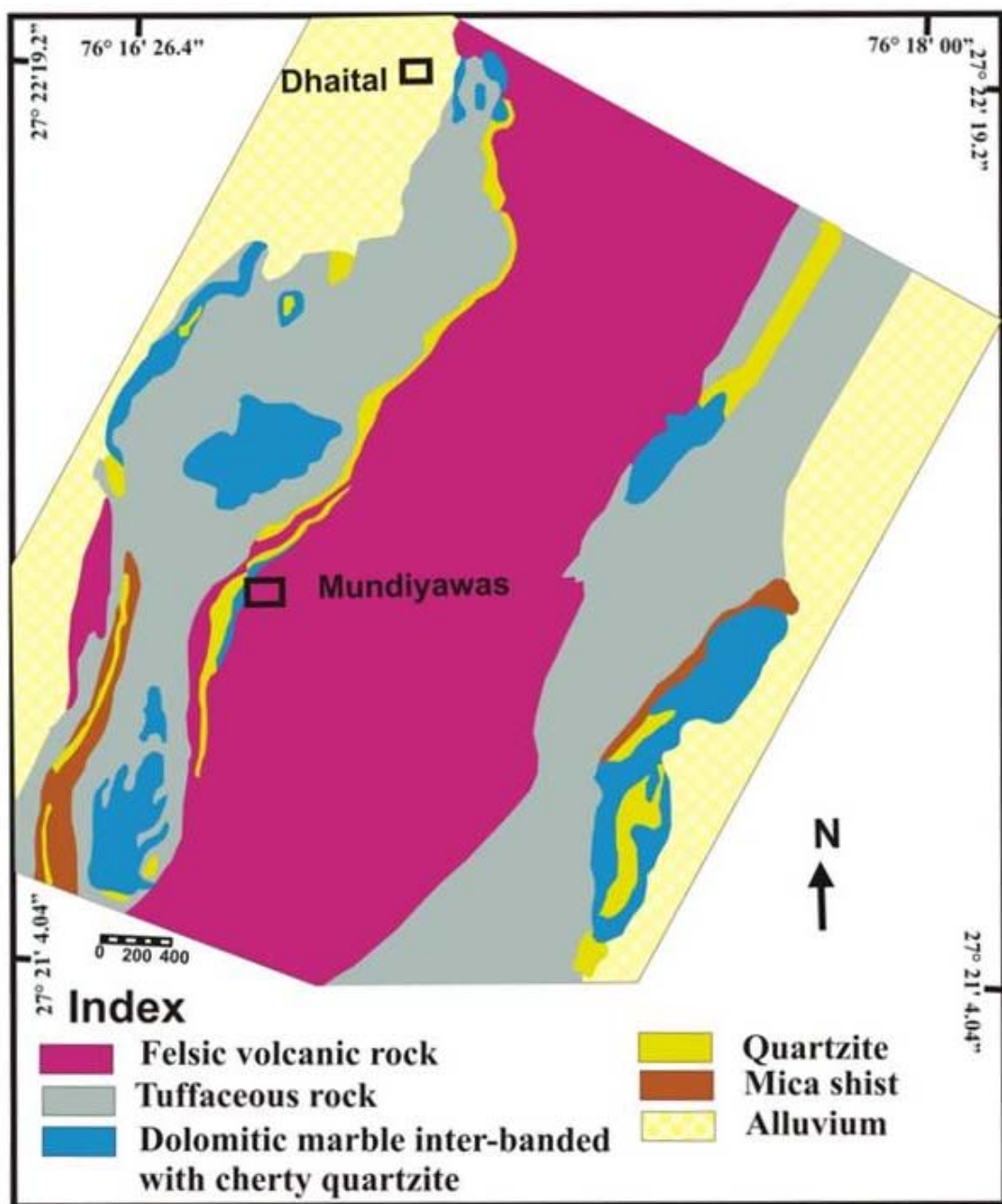


**Figure 3.** Simplified geological map of the study area (Mundiyawas-Khera area) (modified after [14,51]). Mundiyawas and Dhaital are two localities around the deposit and shown in the map.

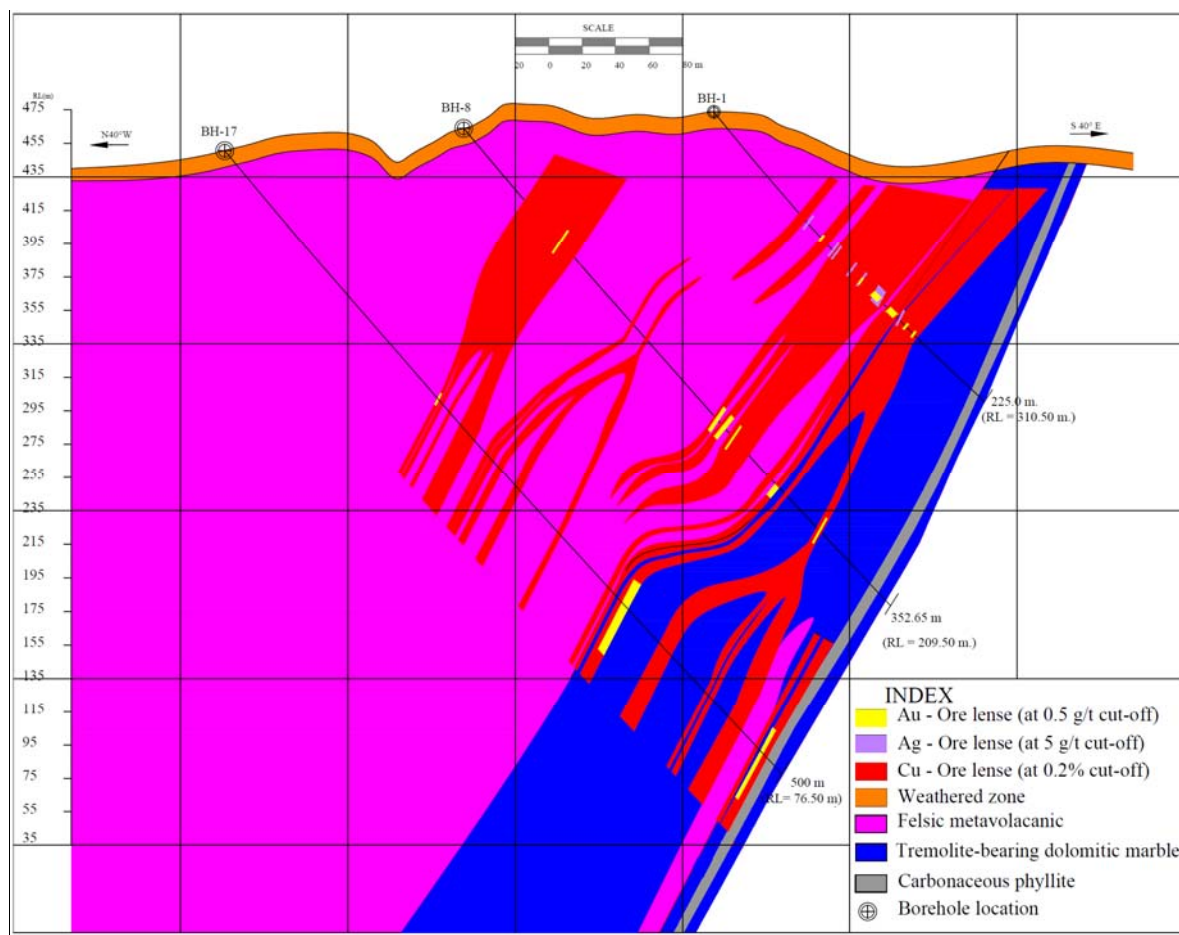


**Figure 4.** Sectional view of host and ore zones intersected along boreholes in the study area after [52].

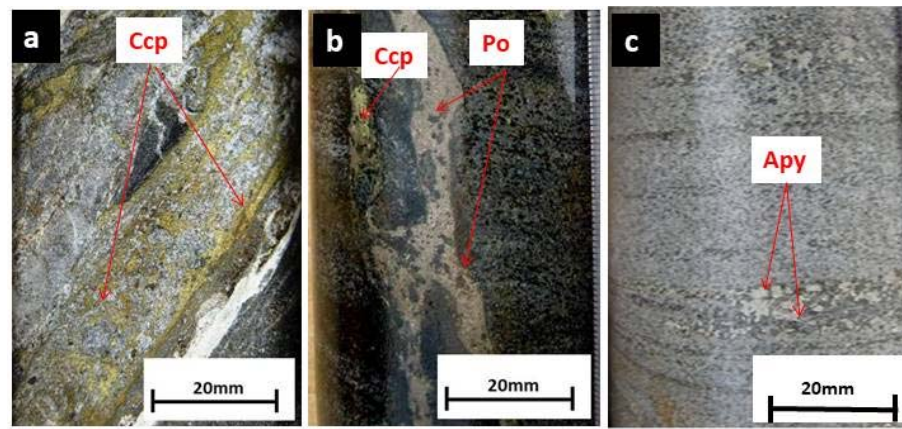


**Figure 5. Cont.**

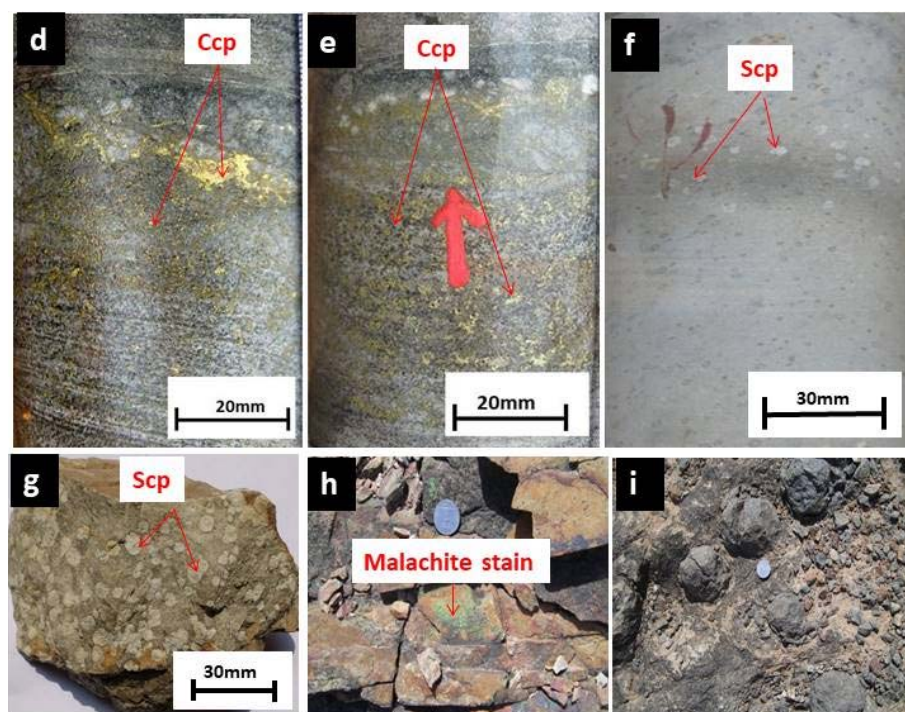


**Figure 5.** Field photographs showing (a) foliation parallel and vein (quartz-carbonate) filled chalcopyrite in felsic meta-volcanic rock; (b) pyrrhotite and chalcopyrite occurring as veins within felsic volcanic rock; (c) arsenopyrite as layers within the coarse grained felsic volcanic rocks; (d,e) stringers and disseminations of chalcopyrite in the coarse grained altered part of the meta-volcanic rock; (f) scapolite (white patches) in the highly altered felsic tuff; (g) scapolite (as white patches) in the fine grained and pervasive felsic volcanic rock; (h) Surficial malachite stains on volcanic tuff; (i) spheroidal weathering exhibited by rhyolite. (Apy: Arsenopyrite, Ccp: Chalcopyrite, Po: Pyrrhotite and Py: Pyrite).

### 3. Material and Methods

Polished thin sections of individual lithology collected from surface and boreholes were studied by Leica DM 27 microscope for understanding the mineralogy as well as textural properties. The whole rock chemical analyses of the representative fresh samples were carried out at National Geophysical Research Institute (NGRI), Hyderabad, India using both XRF (Philips PW-2440 Magix-PRO, The Netherlands) and ICPMS (Perkin Elmer ELAN DRC II, Waltham, MA, USA). Trace elements and REEs were determined by digestion of powder samples by adopting standard operation procedure followed in [53]. JR-1, JR-2 and RGM-1 reference standards were used for the analysis of rhyolite. Precision and accuracy are better than RSD 3% for major oxides and trace elements. Stable isotope (C and O) geochemistry of fresh carbonate veins was done to determine the condition, environment of formation and deposition of ore bearing fluids. Powdered carbonate samples were analyzed using a Kiel IV Carbonate device coupled with a MAT-253 isotope ratio mass spectrometer (IRMS) in dual inlet mode (Thermo Fisher Scientific, Waltham, MA, USA) at Indian Institute of Science Education and Research (IISER) Kolkata. The reference gas ( $\text{CO}_2$ ) used during the analysis of the samples has  $\delta^{13}\text{C}$  and  $\delta^{18}\text{O}$  value of 4.5‰ and 14.05‰, respectively and was calibrated using NBS-19. In the present study, the in-house standard (Z-Carrara Marble, acquired from Physical Research Laboratory, Ahmedabad) was run along with the international standard (NBS-18) to monitor the isotopic composition of the measured samples regularly. The Z-Carrara Marble was calibrated via NBS-18 prior to the analysis of the samples.

## 4. Results

### 4.1. Host Rock and Ore Petrography

A variety of felsic volcanic rocks is observed in Mundiyawas-Khera area with distinct features like tuffaceous, massive, fine grained and coarse grained nature associated with the meta-sediments viz., carbonaceous phyllite and minor dolomite (Figure 5a–i). The coarse grained rhyolite shows spheroidal weathering on the surface at places (Figure 5i). Rounded elliptical scapolite grains within the felsic tuff and felsic meta-volcanic rocks (Figure 5f,g) suggest prominent hydrothermal alteration in the area. The rock is mainly composed of quartz, K-feldspars, biotite, sericite, and minor muscovite (Figure 6a–h). The feldspar grains are euhedral and larger in size. Embayment of quartz and feldspar phenocryst (Figure 6a,b,d,e) are frequently seen in the volcanic rocks, suggesting the volcanic origin [14]. Apart from this, microscopic study reveals intense sericitization (Figure 6a–c) and scapolitization (Figure 6g). A large variation in the grain sizes is observed in felsic meta-volcanic rocks. In some sections, the rock is very fine grained, i.e., cryptocrystalline in nature and individual minerals are difficult to identify (Figure 6f) and have glassy appearance. Although the rocks have suffered metamorphism, interlocking texture between the grains indicate igneous origin. The textural features and mineralogy infer this rock as a felsic volcanic rock.

Textural-microstructural features and ore petrography of different litho-units from the study area confirm the presence of chalcopyrite, pyrrhotite, arsenopyrite and pyrite as the major sulfide mineral phases (Figure 7a–e). However, chalcopyrite is found to be the most dominant copper ore mineral either occurring as fine disseminations within the felsic meta-volcanic rocks and dolomite or as vein fillings (Figure 7a–f). Mutual equilibrium boundary between pyrrhotite and chalcopyrite (Figure 7b,d) suggests the simultaneous crystallization.

### 4.2. Geochemistry of Felsic Volcanic Rocks

The host rock geochemistry has been carried out principally to establish the chemical variations of the felsic meta-volcanic rocks and their bearing on mineralization. Major element data of felsic volcanic rocks (Table S1) show that they have high silica content ranging from 61 to 80 wt% (average: 70%), and low  $\text{Al}_2\text{O}_3$  ( $\text{Al}_2\text{O}_3 < 19\%$ ; average: 13%), low  $\text{MgO}$  (<2%; average: 1%) and high  $\text{FeO}_{\text{T}}$  (4–20%; average: 6%) contents. Major oxide variations plot of the felsic volcanic rocks from Mundiyawas-Khera area with respect to  $\text{SiO}_2$  exhibit decreasing trends for  $\text{Al}_2\text{O}_3$ ,  $\text{MgO}$ ,  $\text{TiO}_2$ ,  $\text{Fe}_2\text{O}_3$  and  $\text{K}_2\text{O}$  (Figure 8). These binary variation patterns suggest fractional crystallization during the evolution of the magma whereas the felsic volcanic shows increasing trend of  $\text{Na}_2\text{O}$  with increasing  $\text{SiO}_2$  content. Total Alkali vs. Silica (TAS) plot (Figure 9a) and  $\text{Nb}/\text{Y-Zr}/\text{TiO}_2$  plot (Figure 9b) confirms the rhyolite-dacite composition of the felsic volcanic rocks. The felsic volcanic rocks show calc-alkaline affinity (Figure 9c) and are metaluminous to peraluminous in nature; however, most of the samples fall in peraluminous field (Figure 9d). The felsic volcanic rock samples of Mundiyawas-Khera area contain some of the highest HFSE and REE contents, hosting VMS-deposits, compared to any other in the world [54,55]. The Zr (86–262 ppm; average 156 ppm), Y (21–68 ppm; average: 34 ppm) and Nb (5–21 ppm; average: 16 ppm) contents are displayed in (Table S1; Figure 9e). Trace element signatures and high Ga/Al ratios are similar to I & S type felsic rocks (Figure 9f).

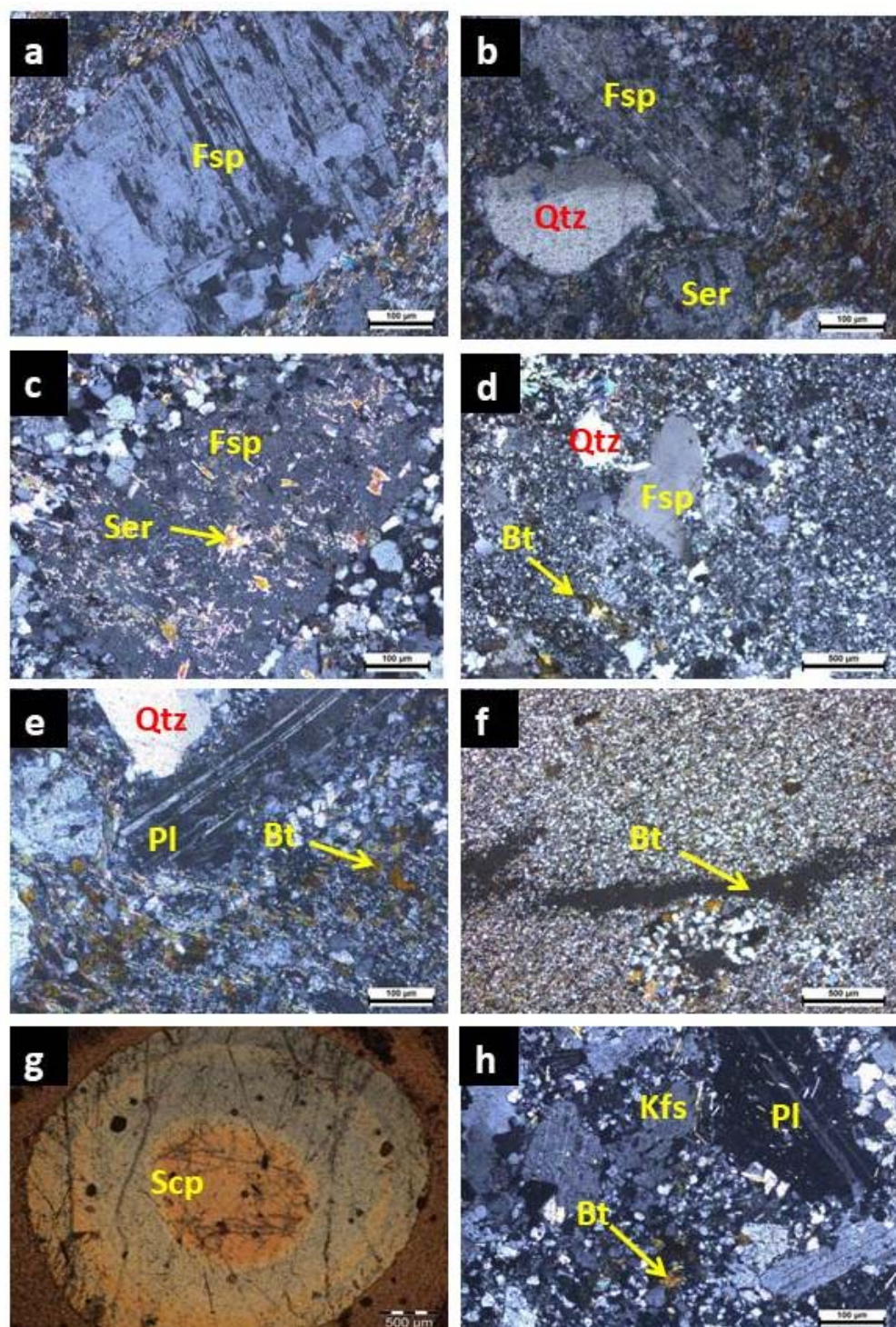


**Figure 6.** Photomicrographs showing (a) phenocryst of feldspar within the siliceous ground mass; (b) phenocrysts of feldspar and quartz showing corrugated margin; (c) sericitization of the feldspar grains observed in the felsic rock intersected; (d) embayment of quartz and feldspar; (e) foliation plane defined by the alignment of biotite and felsic ground mass in the volcanic rock; (f) Segregation of biotite within felsic ground mass; (g) large circular scapolite grain showing in the felsic tuff; (h) feldspar laths showing intergranular texture surrounded by biotite rich groundmass. (Bt: Biotite, Fsp: Feldspar, Kfs: K-feldspar, Pl: Plagioclase feldspar, Scp: Scapolite, Ser: Sericite and Qtz: Quartz).

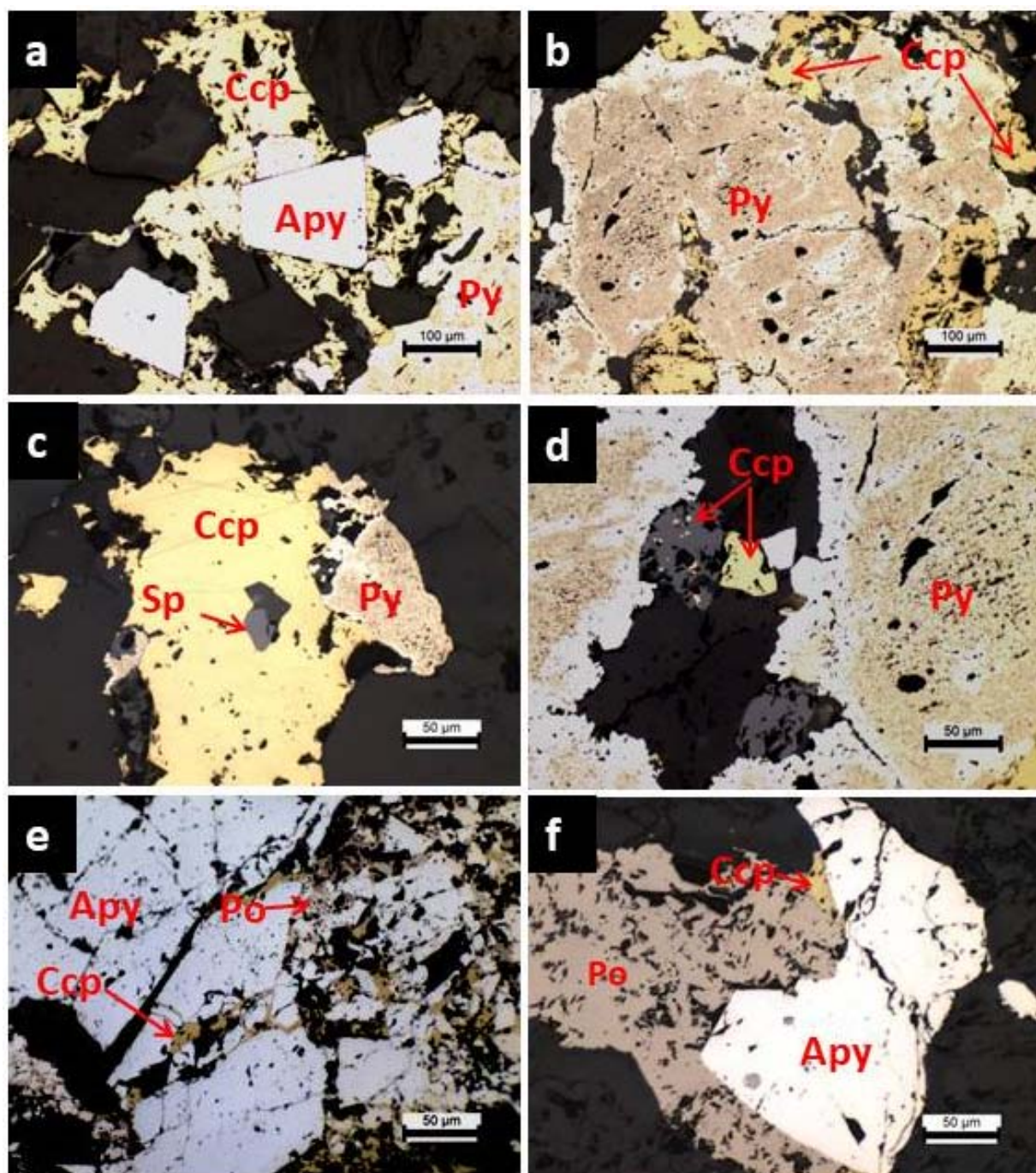


**Figure 7.** Photomicrographs showing association of different generations of mineral assemblages and textural characteristics (a) euhedral arsenopyrite within chalcopyrite grains as disseminated mineralization; (b,c) replacement of chalcopyrite along the fractures of pyrite; laths of chalcopyrite within pyrite; (d) a small grain of sphalerite within chalcopyrite and pyrite present at the outer rim of chalcopyrite; (e) fractured filled pyrrhotite and chalcopyrite in arsenopyrite; (f) coexistence of pyrrhotite-chalcopyrite and arsenopyrite in the mineralized quartz carbonate veins. (Apy: Arsenopyrite, Ccp: Chalcopyrite, Po: Pyrrhotite, Py: Pyrite and Sp: Sphalerite).

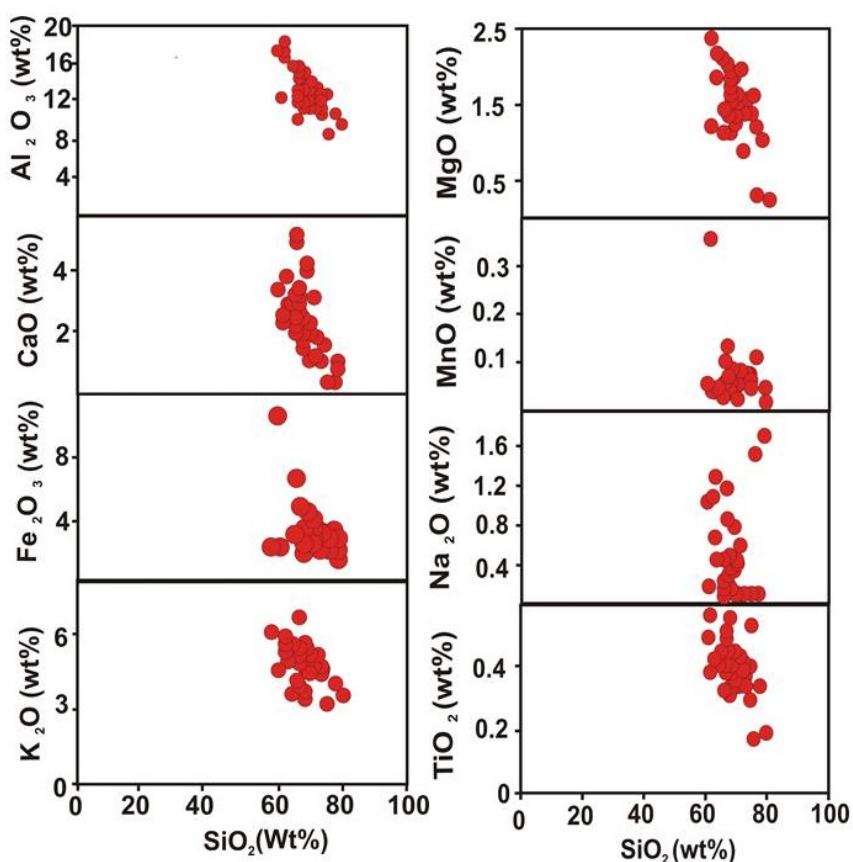


**Figure 8.** Harker variation diagrams for major oxides vs.  $\text{SiO}_2$  contents for the felsic volcanic rocks from Mundiawas-Khera area. (Data source: Table S1).

#### 4.3. Alteration

Hydrothermal alteration is a common phenomenon in many ore deposits and plays a pivotal role in categorizing the deposits according to the characteristic mineral distribution pattern. Here the alteration impressions have been identified both from the megascopic and microscopic characteristics of the host rocks coupled with the host rock geochemistry. Detailed petrographic studies of host rocks around the mineralized zones revealed the occurrences of sericite, scapolite, epidote, calcite and sulfide minerals. However, sericitization (Figure 6b,c) and scapolitization (Figure 6g) were intensely developed in the form of dominant assemblages as compared to other alteration assemblages in the study area. Carbonate occurrences in the form of calcite are very common within host rocks. Crisscross thick and thin vein and veinlets of quartz-carbonate veins and their interrelation with sulfide mineralization clearly suggest repetitive remobilization and redeposition of sulfide minerals due to intense hydrothermal activities. Intricate association of sulfide with scapolite clearly indicates the strong involvement of a hydrothermal fluid for the formation of scapolite. Lithogeochemical characteristics of host rocks are also examined to understand the hydrothermal and digenetic trend in alteration box plot of [61]. The alteration box plot is considered to be a robust method to understand the intensity of alteration suffered by hydrothermal fluids in VMS system [62]. On alteration box plots, felsic volcanic samples of Mundiawas-Khera prospect show four distinct hydrothermal alteration trends (Figure 10). In the alteration box plot (Figure 10), there is a strong correlation towards sericite node (Trend 1). It shows weak sericite alteration at the margins of a hydrothermal system and relatively weak correlation towards sericite-chlorite-pyrite node (Trend 2), chlorite-pyrite-(sericite) node (Trend 3) and carbonate-sericite node (Trend 5). These are clearly discernible with the field and petrographic observations in the study area and are in conformity with other VMS deposits.

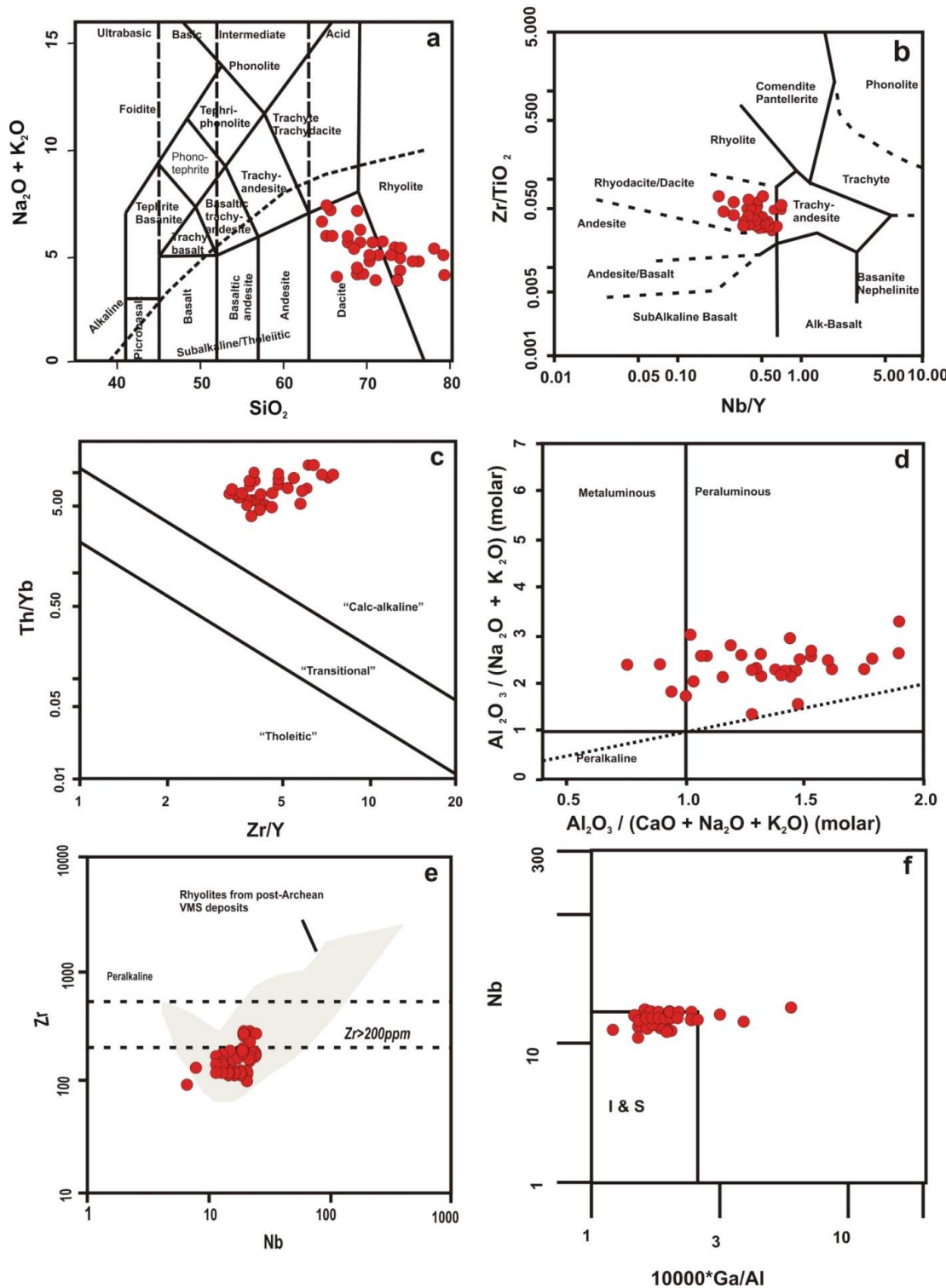


**Figure 9.** Felsic volcanic rocks from Mundiawas-Khera copper deposit plotted against the discrimination diagram: (a) Total Alkali vs. Silica (TAS) plot after [56] show within rhyolite and dacite field; (b) Zr/TiO<sub>2</sub> discrimination diagram of [57] plot well within the rhyo-dacite/dacite field; (c) Th/Yb vs. Zr/Y plot after [58] show calc-alkaline affinity; (d)  $\text{Al}_2\text{O}_3 / (\text{Na}_2\text{O} + \text{K}_2\text{O})$  (molar) vs.  $\text{Al}_2\text{O}_3 / (\text{CaO} + \text{Na}_2\text{O} + \text{K}_2\text{O})$  (molar) plot shows a meta-aluminous to peraluminous character [59]; (e) Zr vs. Nb diagram showing similarities with rhyolites from post-Archean VMS deposits. The Zr-Nb diagram illustrates the HFSE variations in rhyolitic rocks associated with VMS environments [60]; (f) Nb vs. Ga/Al, all sample plots in the I & S-type except a few falling in A-type granite field [61]. (Data source: Table S1).

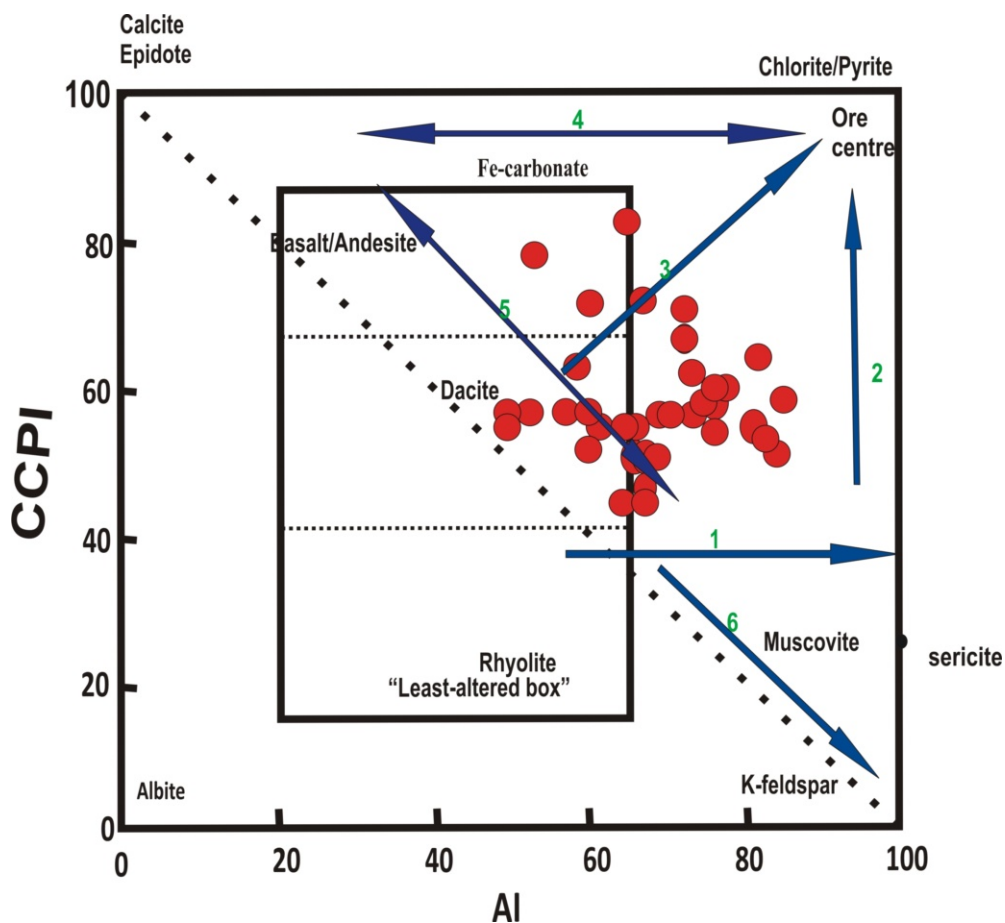


**Figure 10.** Felsic volcanic rocks plotted in the Alteration Box Plot [61] using Alteration Index (AI) versus chlorite–carbonate–pyrite index (CCPI), which shows a strong correlation with Trend 1 and weak correlation with Trend 2, 3 and 5.  $AI = 100 \frac{(K_2O + MgO)}{(K_2O + MgO + Na_2O + CaO)}$ ;  $CCPI = 100 \frac{(MgO + FeO)}{(MgO + FeO + Na_2O + K_2O)}$ . (Data source: Table S1).

#### 4.4. Carbon and Oxygen Isotope Geochemistry of Carbonates

The values of carbon and oxygen isotope depend upon the environment of deposition and are restricted to a particular set of geological reservoirs [63–67]. The carbon and oxygen isotope data of the mineralized carbonate veins from the deposit is given in Table 1. The C and O isotope data are plotted on  $\delta^{13}C_{PDB}$  versus  $\delta^{18}O_{SMOW}$  plot to understand the geological environment of deposition; at the same time, they are also compared with various well-known VMS deposits (Figure 11). The plot shows that the variation of  $\delta^{13}C$  values range between  $-10.4\text{‰}$  and  $-0.9\text{‰}$  ( $\text{min} = -10.6\text{‰}$ ,  $n = 27$ ), whereas the  $\delta^{18}O$  values show a range of  $16.35\text{‰}$  to  $25.23\text{‰}$  ( $\text{min} = 21.49\text{‰}$ ,  $n = 27$ ). The C and O isotopic data of the mineralized carbonate veins of Mundiyawas-Khera copper deposit (Figure 11) does not match with the other carbonate sources and rules out its formation from a single geological environment. Rather, we can propose mixed types of geological environments responsible for the mixing of fluids or this could be due to fluid/rock interactions.

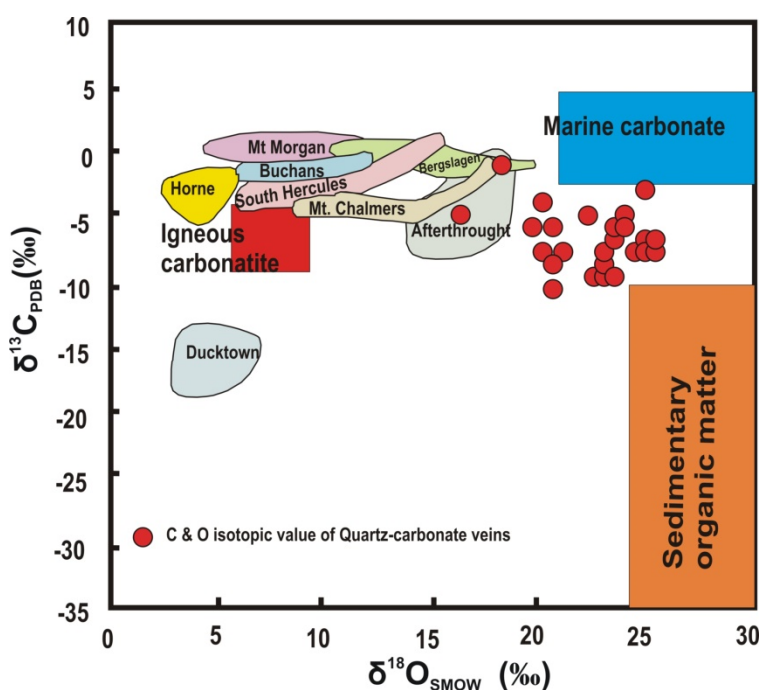


**Figure 11.** Carbon and oxygen isotopic values of quartz-carbonate veins from the Mundiyawas-Khera copper deposit plotted over carbonates of various VMS deposits. Data of major geologic reservoirs are from [63–66] (modified after [67,68]) and other VMS deposits from [69]. It is noted that some of the Mundiyawas-Khera quartz-carbonates overlap on Afterthought, Mt. Chalmers and Bergslagen carbonate fields. Data source as listed in Table 1.

**Table 1.** Carbon and oxygen isotope data from mineralized carbonate vein samples from Mundiyawas-Khera copper deposit.

Sample	Sample Description	δ¹⁸O_SMO	δ¹³C_PDB
KBH-1	Carbonate Vein	20.62152	-10.4
KBH-6	Carbonate Vein	20.75554	-7.6
KBH-8A	Carbonate Vein	23.33281	-9.2
KBH-13	Carbonate Vein	20.21946	-8
KBH-8B	Carbonate Vein	23.74518	-9.8
KBH-18A	Carbonate Vein	24.33279	-7.5
KBH-18B	Carbonate Vein	22.55963	-9.7
KBH-19A	Carbonate Vein	16.35355	-4.6
KBH-19B	Carbonate Vein	25.22969	-2.7
KBH-22A	Carbonate Vein	24.39465	-7.8
KBH-21	Carbonate Vein	25.4771	-6.9
KBH-22B	Carbonate Vein	23.83796	-5.9
KBH-23	Carbonate Vein	20.61121	-8.4
KBH-25	Carbonate Vein	19.88957	-5.4
KEBH-1	Carbonate Vein	23.72456	-9.1
KBH-25B	Carbonate Vein	18.32259	-0.9
KEBH-6A	Carbonate Vein	20.84832	-7.7
KEBH-6B	Carbonate Vein	23.4359	-6.9
KEBH-9A	Carbonate Vein	23.31219	-8.9
KEBH-9B	Carbonate Vein	23.37405	-9.8
KEBH-12A	Carbonate Vein	24.07507	-4.4
KEBH-12B	Carbonate Vein	24.55959	-7.3
KEBH-12C	Carbonate Vein	23.13694	-8.2
KEBH-12B	Carbonate Vein	23.34312	-9.1

**Table 1.** *Cont.*

Sample	Sample Description	$\delta^{18}\text{O}_{\text{SMOW}}$	$\delta^{13}\text{C}_{\text{PDB}}$
KEBH-12E	Carbonate Vein	20.53905	-5.9
KEBH-12F	Carbonate Vein	20.13699	-3.7
KEBH-12H	Carbonate Vein	22.39468	-4.9
KEBH-12I	Carbonate Vein	22.48747	-9.5

The solubility of carbonate is directly proportional to pressure and inversely proportional to temperature [70]. Hence, we cannot expect the precipitation of calcite from a hydrothermal solution by simple cooling under a closed system. The promising conditions for precipitations of carbonates from a hydrothermal fluid are either degassing of CO<sub>2</sub> from the fluid or processes like boiling and change in pH [71]. The nearly horizontal negative correlation array could be due to the isotopic composition of oxygen in the fluid remaining unchanged, but the isotopic composition of carbon was changed due to the loss of CO<sub>2</sub> and leads to an increase in pH of the fluid and a change in dissolved carbon species from H<sub>2</sub>CO<sub>3</sub> to HCO<sub>3</sub> [71]. This isotopic variation of carbonates is due to the crystallization from a mixed carbon species and in a transitional condition [71,72]. The inter-relationship between the  $\delta^{18}\text{O}$  values and temperature of hydrothermal fluids and the wide range of variations from 7.5 to 20.0‰ is interpreted as a result of varying depositional temperatures ranging between 100 °C and 300 °C [73]. In Mundiyawas-Khera copper deposit, the  $\delta^{18}\text{O}$  values are a little on the higher side with respect to the mentioned deposits in Figure 9 and vary in the range of 16.35‰ to 25.23‰ (min = 21.49‰, n = 27).

## 5. Discussion

### 5.1. Felsic Volcanic Rock Classification and Petrogenesis

On the basis of petrochemical signature, felsic volcanic rocks are divided into four classes, e.g., FI, FII, FIII and FIV [55,74–76]. The FI felsic volcanic rocks are characterized by steep REE patterns, weakly negative to moderately positive Eu anomalies and high Zr/Y and low abundances of high field strength elements (HFSE, Y, Zr, Hf); FII felsic volcanic rocks are characterized by gently sloping REE patterns, variable Eu anomalies, moderate Zr/Y and intermediate abundances of HFSE; FIII felsic volcanic rocks, rhyolites and high silica rhyolites, are characterized by relatively flat REE patterns and subdivided into two types. The sub-type FIIIa rhyolites exhibit variable negative Eu anomalies, low Zr/Y and intermediate abundances of HFS elements. FIIIb rhyolites exhibit pronounced negative Eu anomalies, low Zr/Y and high abundances of HFSE. FIV felsic volcanic rocks are rhyolites and high silica rhyolites characterized by flat to slightly LREE-depleted REE patterns and low REE and HFSE abundances [76]. This classification of felsic volcanic rocks is mainly dependent on the type of crust in which they are sustained (i.e., evolved or juvenile) and are invariably a function of age (i.e., Archean or post-Archean). The analyzed samples dominantly fall in FIIIa, FIV and FII of rhyolite discrimination diagram (Figure 12a) and suggest that the felsic volcanic rocks are probably evolved due to the partial melting of crust at shallow to moderate depths (<15 km) [75,76]. From Zr/Y vs. Y plot (Figure 12b), the felsic volcanic samples fall in the FII and FIIIa field suggesting moderate to most prospective area of Archean VMS deposits [77]. The felsic volcanic rocks of Mundiyawas-Khera prospect have chemical characteristics consistent with an arc related rifted continental margin setting and are characteristic to VAG (Volcanic Arc Granite) and WPG (Within Plate Granite) after tectonic discrimination diagrams (Figure 12c) of [78] for granitoid rocks. In the Nb-Y plot, the felsic rocks have a trend towards syncollisional granite and within plate granite in an evolved arc setting (Figure 12d). The Th/Yb vs. Nb/Yb plot (Figure 12e) of [79] suggests volcanic arc array field and in Rb/Nb vs. Y/Nb diagram (Figure 12f) felsic volcanic samples show A2, crustal derived granitoid rocks [80].

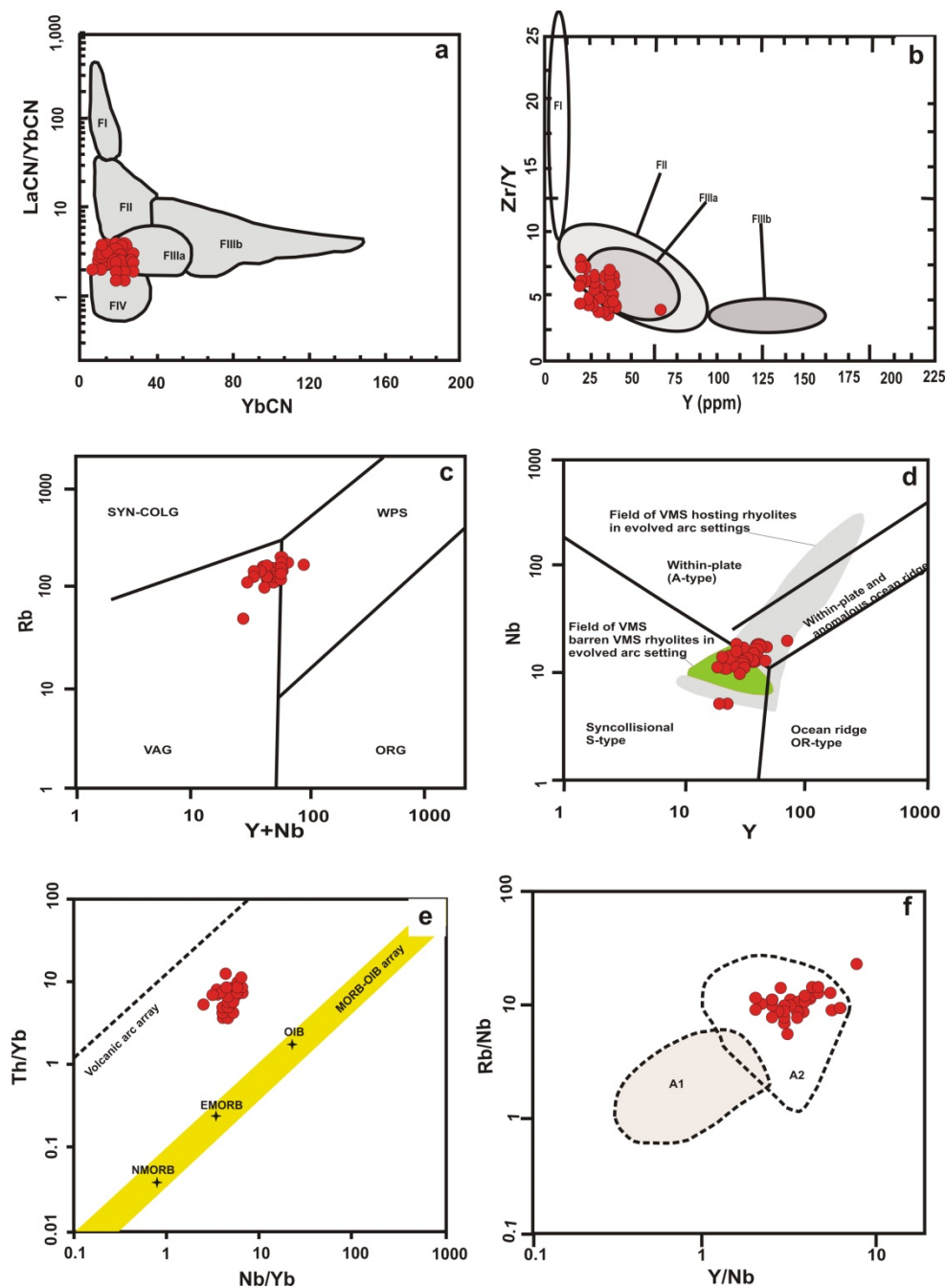


**Figure 12.** Petrochemical affinity of the felsic volcanic rocks (a) Chondrite normamilized [81]  $\text{La}_{\text{CN}}/\text{Yb}_{\text{CN}}$  vs  $\text{Yb}_{\text{CN}}$  rhyolite discrimination diagram after [75,76]; most of the felsic rocks show FIIIa affinity and a few show FII and FIV affinities; (b)  $\text{Zr}/\text{Y}$  vs.  $\text{Y}$  diagram of [75], as modified by [55], with magmatic affinities based on  $\text{Zr}/\text{Y}$  ratios from the concepts of [82]; most of the felsic rocks have FIIIa to FII affinity; (c)  $\text{Rb}$  vs.  $\text{Y} + \text{Nb}$  tectonic discrimination diagrams of [78] for granitoid rocks and samples show VAG (Volcanic Arc Granite) and WPG (Within Plate Granite) (d)  $\text{Zr}$  vs.  $\text{Nb}$  plot shows that the felsic volcanic rocks are HFSE-enriched and support the evolved arc setting after [83]: the fields of VMS-barren (green shaded color) and VMS-hosting rhyolites (grey shaded color) in post-Archean continental crust-associated setting. The shaded fields are from [83]. The sample falls on the syncollisional S-type granite and within plate granite. (e)  $\text{Th}/\text{Yb}$  vs  $\text{Nb}/\text{Yb}$  plot is from [79]. The sample falls on volcanic arc array field (f)  $\text{Rb}/\text{Nb}$  vs  $\text{Y}/\text{Nb}$  diagram, A1, mantle derived and A2, crustal-derived granitoid rocks [80]; felsic volcanic samples fall in A2, which shows crustal derivative signature. (Data source: Table S1).

Trace element compositions of felsic meta-volcanic rocks are marked by lower concentrations of compatible elements such as Ni, Cr and enrichment of large ion lithophile elements (LILE) over high field strength elements (Table S1). Chondrite-normalized REE pattern [84] of the felsic volcanic rock/tuff suggests a considerable LREE/HREE fractionation trend with negative Eu anomalies (Figure 13a). The depleted and flat HREE pattern again indicates crustal source that was garnet free. A negative Eu anomaly is typical of many continental rocks and probably arises because many crustal rocks were produced by intracrustal partial melting. The residue of these melts was rich in plagioclase, hence retaining more Eu in the lower crust and creating a complimentary Eu-depleted upper crust. Negative Eu anomaly also points to cooler fluids, more oxidized condition and/or increased clastic contributions [85]. The primitive mantle-normalized after [86] trace element pattern (Figure 13b) of the felsic volcanic rock shows distinct negative Nb, Zr and Ti anomalies. Enrichment of LILE (e.g., Cs, Rb, Ba, Th and U) and depletion of HFSE (e.g., Zr, Nb and Ti) relative to typical primitive mantle values with negative Nb, Zr and Ti anomalies and positive Th anomalies is suggestive of a subduction zone magma character generated in arc settings [78].

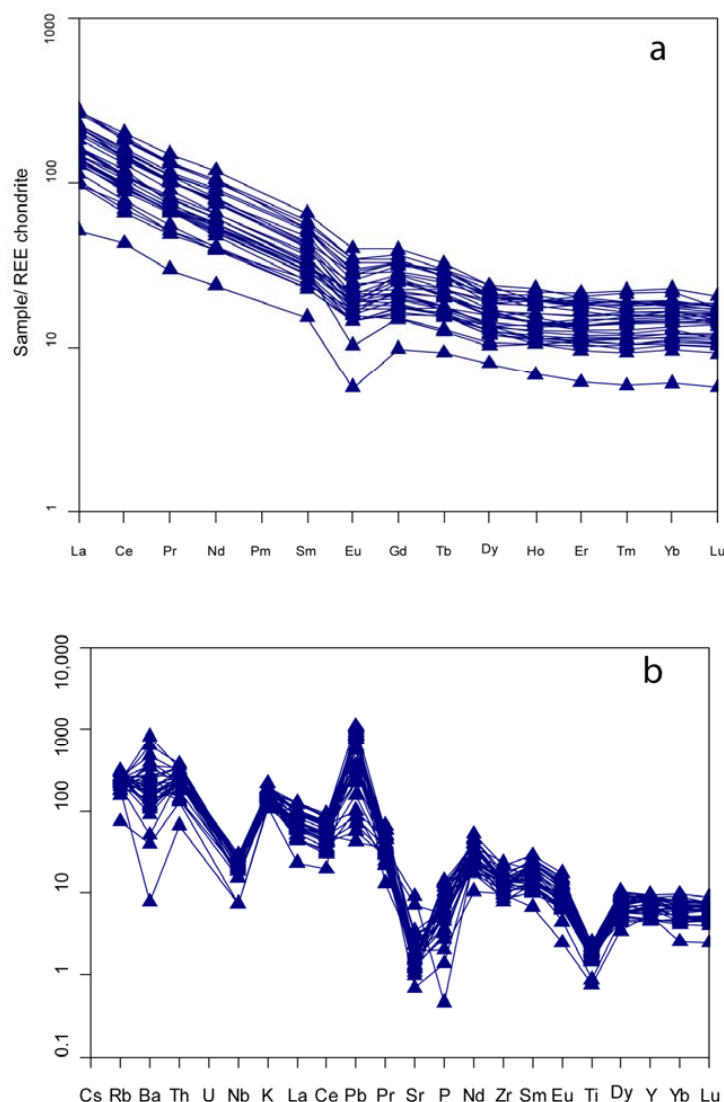


**Figure 13.** (a) Chondrite-normalized rare earth element (REE) plots [84]; and (b) Primitive mantle normalized spider plot of trace element [86] of the felsic volcanic rocks from the study area. (Data source: Table S1).

## 5.2. Source and Evolution of Ore Fluids

The isotopic results indicate the dominancy of highly modified sea water after infiltration into the upper crust, interaction with the underlying volcanic and sedimentary rocks and convective circulation to the venting sites. This model is in favor of the ancient and modern hydrothermal system models of massive sulfide formation [87–92]. The interpretations of isotopic data (Figure 11) suggest a minor participation of magmatic carbonate in the genesis of mineralized carbonate veins in Mundiyawas-Khera copper deposit. As suggested by [93], in Neves-Corvo deposit, magmatism plays an important role, not only as a driving force of seawater convection but also as a direct contributor of metals and volatile components to the hydrothermal systems. This model may be considered to explain the genesis of ore bearing hydrothermal fluid in Mundiyawas-Khera copper deposit from carbon and oxygen isotope study.

## 5.3. Tectonic and Structural Setting

The lithogeochemistry of felsic volcanic rocks reveals arc magmatic signature (Figure 12c,d). In addition, the FII, FIIIa and FIV signatures (Figure 12a) of the felsic volcanic rocks suggest that they could be evolved from the partial melting of crust at shallow to moderate depths due to subvolcanic eruptions [75,76]. The arc signature of Mundiyawas-Khera felsic volcanic rocks could be correlated with the arc magmatism in NDFB [94,95] and a probable geodynamic model (Figure 14) is proposed to understand the possible massive sulfide deposit of Mundiyawas-Khera area.

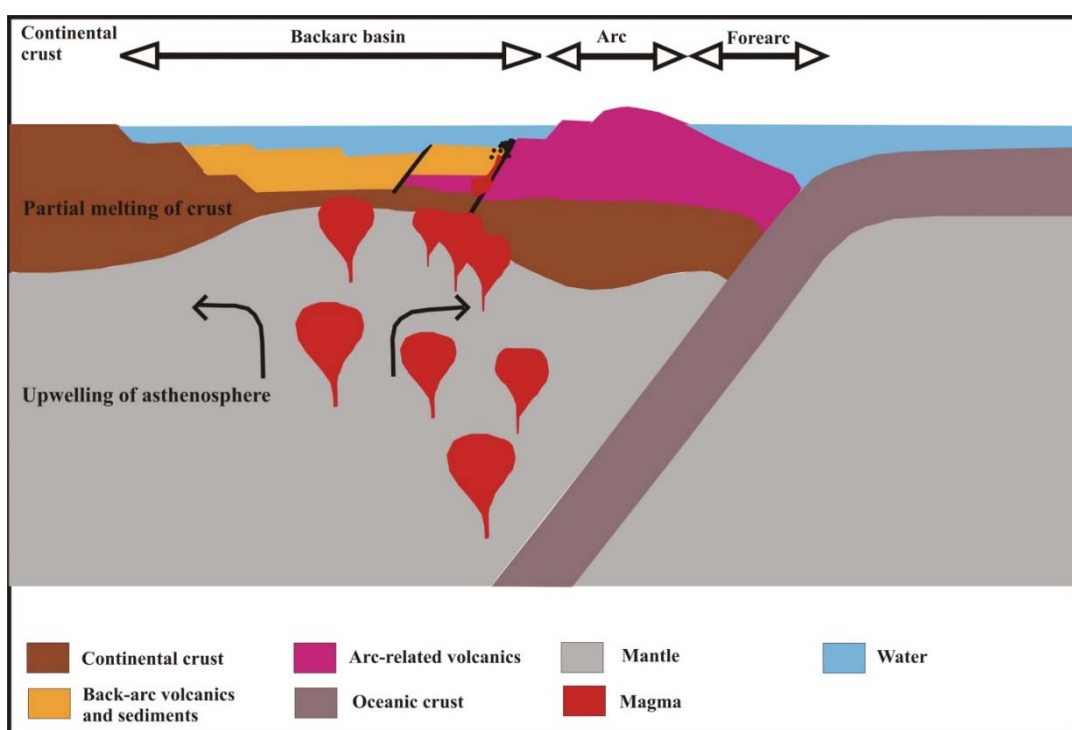


**Figure 14.** Schematic geodynamic model showing possible massive sulfide deposit of Mundiyawas-Khera copper deposit, i.e., Upwarping and rifting of continental crust due to upwelling of magma from asthenosphere in a back arc basin and partial melting of continental crust, disseminated sulfides (pyrite, pyrrhotite, chalcopyrite and arsenopyrite) deposit with syn-volcanic eruption and epigenetic copper mineralization due to circulation of hydrothermal fluids.

## 5.4. A VMS Perspective of Mundiyawas-Khera Copper Deposit

A number of VMS prospects in India are comprised of mafic, mafic-siliciclastic, bimodal mafic and bimodal-felsic deposits [96,97]. Cu, Pb and Zn ores are associated with them. The Deri-Ambaji [10], Pipela VMS prospect in western India [96,98] and the Betul

VMS prospect of Central India [97,98] are the established VMS deposits in India. The detailed characteristics are given in Table 2. A thorough understanding of the nature of mineralization in the Mundiyawas-Khera copper deposit would provide key aspects on exploration strategies. From the stable isotope (C & O) geochemistry, the deposit is more likely to be an IBP deposit [92], similar to Afterthoughts VMS deposit, Mt. Chalmers and Bergslagen VMS deposits [73]. The lithogeochemical classifications of felsic volcanic rocks reveal; FII, FIIIa and FIV affinity and similarity to FII felsic volcanic rocks (Sturgeon Lake, Kuroko, Rio Tinto, Bathurst, Myra Falls, Mt. Chalmers, Mt. Windsor, Tulsequah Chief, Thalanga, Mt. Read, Boliden, Selbaie, Salt Creek), FIIIa felsic volcanic rocks (Noranda, Jerome, United Verde, Teutonic Bore, Parys Mountain, Ambler, Avoca, Woodlawn, Buchans, Prieska, Fox Lake, Manitouwadge, Hood river, Sulfur Springs, Scuddles, Berslagen, Winston Lake) and FIV felsic volcanic rocks (Snow lake, FlinFlon, West Shasta, Kutcho Creek, Canatuan) according to [76]. Presence of alteration mineral assemblages have close similarities with the VMS type deposit [99,100]. From the lithogeochemistry, tectonic setting and felsic volcanic classification point of view, we inferred the Mundiyawas-Khera copper deposit shares similarities with the VMS deposit of Nohkouhi, Post e Badam block, Central Iran [74].

**Table 2.** A comparison status of felsic volcanic hosted VMS deposit in a global scenario with similarities and dissimilarities in lithological, mineralogical and tectonic framework.

Deposit	Style	Age	Host Rock	Ore Minerals	Ore	Tectonic Setting/ Interpreted Environment	Deposit Type	Hanging Wall Alteration	References
Mt. Lyell	Lenses	Cambrian	Quartz-sericite-pyrophyllite schist, rhyolitic-andesitic volcanic rocks	Pyrite, chalcopyrite, bornite, galena and sphalerite Pyrrhotite, pyrite, chalcopyrite, sphalerite, galena, and magnetite	Cu, Pb, Zn and Au Au-Cu rich but Zn poor	Convergent plate boundary Extension setting	Subseafloor and sea floor Subseafloor	strong/intense strong	[101,102] [103]
Mattabi	Lenses	Neo-Archean	Rhyolite and andesite	Pyrite, chalcopyrite, galena and sphalerite	Cu, Pb and Zn	Extensional tectonic settings	Subseafloor	strong	[74]
Nohkouhi	Stockwork and Lenses	Late Pre-cambrian to Early Cambrian	Black shale and rhyodacite	Pyrite, chalcopyrite, galena and sphalerite	Cu, Pb and Zn	Arc magmatism	Subseafloor	strong	[96,97]
Pipela	Massive stratiform	Neo-Proterozoic	Chlorite-mica-quartz schist, amphibolite and rhyolite	Pyrite and sphalerite	Cu and Zn	Subseafloor	strong	[96,97]	
Ambaji and Deri	Tabular and lensoid	Neo-Proterozoic	Cordierite-anthophyllite-chlorite rock, amphibolite and rhyolite	Pyrite, sphalerite, galena, chalcopyrite and pyrrhotite	Cu, Pb and Zn	Arc magmatism	Subseafloor	strong	[96,97]
Betul belt	Lenses	Palaeo-Proterozoic	Rhyolite, pillowd basalt, rhyolitic autobreccia, hyaloclasite, peperite and tremolite-carbonate rock	Sphalerite, pyrite, galena and chalcopyrite	Zn-Pb-Cu	continental back-arc rift	Seafloor	strong	[97,104]
Mundiyawas Khera	Dissemination and lenses	Meso-Proterozoic	Felsic volcanic rocks of rhyodacite composition and dolomite	Chalcopyrite, arsenopyrite, pyrrhotite, sphalerite and galena	Cu-Au-Ag-Pb-Zn	Arc magmatism	Subseafloor	strong	[13,14,16–18]

## 6. Conclusions

The Proterozoic felsic volcanic (rholite-dacite composition) hosted copper-gold deposit in Mundiyawas-Khera area is located within the Alwar basin of western India. Presence of ample amounts of scapolite, sericite, epidote and carbonates on felsic volcanic rocks is presumed to be the product of intense fluid–rock interactions, i.e., interactions between host rocks and ore bearing fluids. The lithogeochemical signature of felsic volcanic rocks indicates arc magmatic affinities and calc alkaline composition. FIIIa, FII and FIV type rhyolite found in VMS deposit have been identified in the area. C and O isotope results

of the mineralized carbonate veins from the study area suggest a mixed source of crustal derived ore bearing fluid with deposits in a temperature range of 65 to 150 °C. From the tectonic, style, geology, mineralization and lithogeochemistry of felsic volcanic rocks of Mundiyawas-Khera, copper-gold deposit is classified under VMS type of deposit. This study will serve as a guiding tool to obtain new mineral prospects in the same stratigraphic horizon with similar lithogeochemical assemblages, in the near vicinity of the study area.

**Supplementary Materials:** The following supporting information can be downloaded at: <https://www.mdpi.com/article/10.3390/min12030370/s1>, Table S1: Major and trace element data of the felsic volcanic rocks from Mundiyawas-Khera area. The geochemical data used in the manuscript is attached as Supplementary file.

**Author Contributions:** Conceptualization of the manuscript: J.S., P.R.S., Field data collection: J.S., P.R.S., I.K., Original draft preparation: J.S., P.R.S., Editing and reviewing: A.S.V. All authors have read and agreed to the published version of the manuscript.

**Funding:** The research work is funded by DST-SERB, Govt. of India for financial support to P R Sahoo vide R & D Project No. ECR/2017/003106.

**Data Availability Statement:** Not applicable.

**Acknowledgments:** The authors are thankful to the Director, Indian Institute of Technology (Indian School of Mines), Dhanbad for providing support. We would like to thank the Geological Survey of India (GSI) for extending necessary support during field studies. We acknowledge the Director, CSIR-National Geophysical Research Institute (NGRI), Hyderabad for carrying out the analysis of major oxide, trace elements and REE analysis of the host rocks. We thank Prasanta Sanyal, Indian Institute of Science Education and Research Kolkata for C-O isotope analyses. JS acknowledges the Director General, Geological Survey of India (GSI) for permitting the continuation of the doctoral degree. PRS is thankful to DST-SERB, Govt. of India for financial support from R & D Project No. ECR/2017/003106. We are thankful to the three anonymous reviewers for their constructive suggestions for the improvement in the manuscript.

**Conflicts of Interest:** The authors declare no conflict of interest.

## References

1. Misra, K. *Understanding Mineral Deposits*; Springer Science and Business Media LLC: Berlin/Heidelberg, Germany, 2000; Volume 1, ISBN 978-04-553009-0. [[CrossRef](#)]
2. Laznicka, P. *Giant Metallic Deposits Future Sources of Industrial Metals*, 2nd ed.; Springer Science and Business Media LLC: Berlin/Heidelberg, Germany, 2010; ISBN 978-3-642-12404-4. e-ISBN 978-3-642-12405-1. [[CrossRef](#)]
3. Mudd, G.; Weng, Z.; Jowitt, S.M. A Detailed Assessment of Global Cu Resource Trends and Endowments. *Econ. Geol.* **2013**, *108*, 1163–1183. [[CrossRef](#)]
4. Kojima, S.; Trista-Aguilera, D.; Hayashi, K.I. Genetic Aspects of the Manto-type Copper Deposits Based on Geo-chemical Studies of North Chilean Deposits. *Resour. Geol.* **2009**, *59*, 87–98. [[CrossRef](#)]
5. Dill, H.G. The “chessboard” classification scheme of mineral deposits: Mineralogy and geology from aluminum to zirconium. *Earth-Science Rev.* **2010**, *100*, 1–420. [[CrossRef](#)]
6. Barrie, C.T.; Hannington, M.D. Classification of Volcanic-Associated Massive Sulfide Deposits Based on Host-Rock Composition. *Rev. Econ. Geol.* **1999**, *8*, 1–11. [[CrossRef](#)]
7. Kampmann, T.C.; Jansson, N.F.; Stephens, M.B.; Majka, J.; Lasskogen, J. Systematics of Hydrothermal Alteration at the Falun Base Metal Sulfide Deposit and Implications for Ore Genesis and Exploration, Bergslagen Ore District, Fennoscandian Shield, Sweden. *Econ. Geol.* **2017**, *112*, 1111–1152. [[CrossRef](#)]
8. Sillitoe, R.H. Porphyry Copper Systems. *Econ. Geol.* **2010**, *105*, 3–41. [[CrossRef](#)]
9. Sarkar, S.; Dasgupta, S. Geologic setting, genesis and transformation of sulfide deposits in the northern part of Khetri copper belt, Rajasthan, India? An outline. *Miner. Deposita* **1980**, *15*, 117–137. [[CrossRef](#)]
10. Tiwary, A.; Deb, M. Geochemistry of hydrothermal alteration at the Deri massive sulphide deposit, Sirohi district, Rajasthan, NW India. *J. Geochem. Explor.* **1997**, *59*, 99–121. [[CrossRef](#)]
11. Knight, J. The Khetri copper belt, Rajasthan: Iron-oxide copper-gold terrane in the Proterozoic of NW India. *Hydro-Therm. Iron Oxide Copp.-Gold Relat. Depos. Glob. Perspect.* **2002**, *2*, 321–341.
12. Baidya, A.S.; Sen, A.; Pal, D.C.; Upadhyay, D. Ore-forming processes in the Khetri Copper Belt, western India: Constraints from trace element chemistry of pyrite and CO isotope composition of carbonates. *Mineralium Deposita* **2021**, *56*, 957–974. [[CrossRef](#)]

13. Khan, I.; Rai, D.K.; Sahoo, P.R. A note on new find of thick copper and associated precious metal mineralisation from Alwar basin of North Delhi Fold Belt, Rajasthan. *J. Geol. Soc. India* **2013**, *82*, 495–498. [[CrossRef](#)]
14. Khan, I.; Sahoo, P.R.; Rai, D.K. Proterozoic felsic volcanics in Alwar Basin of North Delhi Fold Belt, Rajasthan: Implication for copper mineralization. *Curr. Sci.* **2014**, *106*, 27–28.
15. Sharma, J.P.; Sahoo, P.R.; Mahanta, H.; Venkatesh, A.; Babu, E.; John, M.M. Constraints on the genesis of the Proterozoic bornite dominated copper deposit from Nim ka Thana, western India: An IOCG perspective. *Ore Geol. Rev.* **2020**, *118*, 103338. [[CrossRef](#)]
16. Khan, I.; Sahoo, P.R. Investigation for copper and associated precious metals in Khera east block, Mundiyawas-Khera area, Alwar district, Rajasthan. *GSI Final Report FS* **2013**, 2012–2013, *Unpublished*.
17. Khan, I. Final report on exploration by deep drilling for copper and associated precious metals in Khera main block, Mundiyawas-Khera area, Alwar district, Rajasthan. *GSI Final Report FS* **2015**, 2014–2015, *Unpublished*.
18. Khan, I.; Siddiqui, S. General Exploration for Copper and associated precious metals in Khera Main block, Mundiyawas-Khera Area, Alwar District, Rajasthan. *Geol. Surv. India Report FS* **2016**, 2015–2016, *Unpublished*.
19. Rao, G.S.; Arasada, R.C.; Sahoo, P.R.; Khan, I. Integrated geophysical investigations in the Mudiyawas–Khera block of the Alwar basin of North Delhi Fold Belt (NDBF): Implications on copper and associated mineralisation. *J. Earth Syst. Sci.* **2019**, *128*, 161. [[CrossRef](#)]
20. Sengar, V.K.; Venkatesh, A.S.; Champatiray, P.K.; Sahoo, P.R.; Khan, I.; Chatteraj, S.L. Spaceborne mapping of hydrothermal alteration zones associated with the Mundiyawas–Khera copper deposit, Rajasthan, India, using SWIR bands of ASTER: Implications for exploration targeting. *Ore Geol. Rev.* **2020**, *118*, 103327. [[CrossRef](#)]
21. Powar, K.; Patwardhan, A. Tectonic evolution and base-metal mineralisation in the Aravalli–Delhi belt, India. *Precambrian Res.* **1984**, *25*, 309–323. [[CrossRef](#)]
22. Heron, A.M. The Geology of Central Rajputana. *Mem. Geol. Surv. India* **1953**, *79*, 389.
23. Roy, A.B.; Kröner, A.; Bhattacharya, P.K.; Rathore, S. Metamorphic evolution and zircon geochronology of early Proterozoic granulites in the Aravalli Mountains of northwestern India. *Geol. Mag.* **2005**, *142*, 287–302. [[CrossRef](#)]
24. Buick, I.; Allen, C.M.; Pandit, M.; Rubatto, D.; Hermann, J. The Proterozoic magmatic and metamorphic history of the Banded Gneiss Complex, central Rajasthan, India: LA-ICP-MS U–Pb zircon constraints. *Precambrian Res.* **2006**, *151*, 119–142. [[CrossRef](#)]
25. Buick, I.; Clark, C.; Rubatto, D.; Hermann, J.; Pandit, M.; Hand, M. Constraints on the Proterozoic evolution of the Aravalli–Delhi Orogenic belt (NW India) from monazite geochronology and mineral trace element geochemistry. *Lithos* **2010**, *120*, 511–528. [[CrossRef](#)]
26. Bhowmik, S.K.; Bernhardt, H.J.; Dasgupta, S. Grenvillian age high-pressure upper amphibolite–granulite meta-morphism in the Aravalli–Delhi Mobile Belt, Northwestern India: New evidence from monazite chemical age and its implication. *Precambrian Res.* **2010**, *178*, 168–184. [[CrossRef](#)]
27. Hazarika, P.; Upadhyay, D.; Mishra, B. Contrasting geochronological evolution of the Rajpura–Dariba and Rampu-ra–Agucha metamorphosed Zn–Pb deposit, Aravalli–Delhi Belt, India. *J. Asian Earth Sci.* **2013**, *73*, 429–439. [[CrossRef](#)]
28. Kaur, P.; Zeh, A.; Chaudhri, N.; Eliyas, N. Two distinct sources of 1.73–1.70 Ga A-type granites from the northern Aravalli orogen, NW India: Constraints from in situ zircon U–Pb ages and Lu–Hf isotopes. *Gondwana Res.* **2017**, *49*, 164–181. [[CrossRef](#)]
29. Gupta, S.N.; Arora, Y.K.; Mathur, R.K.; Iqbaluddin Prasad, B.; Sahai, T.N.; Sharma, S.B. The Precambrian Geology of the Aravalli Region, southern Rajasthan and North-eastern Gujarat. *Mem. Geol. Surv. India* **1997**, *123*, 262.
30. Sinha-Roy, S.; Malhotra, G.; Mohanty, M. *Geology of Rajasthan*; Geological Society of India: Bangalore, India, 1998; 278p.
31. Roy, A.B.; Jakhar, S.R. *Geology of Rajasthan (Northwest India) Precambrian to Recent*; Scientific Publishers: Jodhpur, India, 2002; 421p.
32. Kaur, P.; Zeh, A.; Chaudhri, N. Palaeoproterozoic continental arc magmatism, and Neoproterozoic metamorphism in the Aravalli–Delhi orogenic belt, NW India: New constraints from in situ zircon U–Pb–Hf isotope systematics, monazite dating and whole-rock geochemistry. *J. Southeast Asian Earth Sci.* **2017**, *136*, 68–88. [[CrossRef](#)]
33. Ahmad, T.; Deb, M.; Tarney, J.; Raza, M. Proterozoic mafic volcanism in the Aravalli–Delhi Orogen, north-western India: Geochemistry and tectonic framework. *J. Geol. Soc. India* **2008**, *72*, 93–111.
34. Choudhary, A.K.; Gopalan, K.; Sastry, C.A. Present status of the geochronology of the Precambrian rocks of Rajasthan. *Tectonophysics* **1984**, *105*, 131–140. [[CrossRef](#)]
35. Naha, K.; Halyburton, R. Early Precambrian stratigraphy of central and southern Rajasthan, India. *Precambrian Res.* **1974**, *1*, 55–73. [[CrossRef](#)]
36. Naha, K.; Roy, A. The problem of the Precambrian basement in Rajasthan, western India. *Precambrian Res.* **1983**, *19*, 217–223. [[CrossRef](#)]
37. Sinha-Roy, S. *Proterozoic Wilson Cycles in Rajasthan*; Memoir Geological Society of India: Bangalore, India, 1988; Volume 7.
38. Mukherjee, R.; Venkatesh, A.S. Geochemical characterization of mineralized albite from Paleoproterozoic Bhukia IOCG–IOA deposit of Aravalli–Delhi Fold Belt, Rajasthan, western India: Genetic linkage to the gold ( $\pm$ Cu $\pm$ U) mineralization. *Geol. J.* **2020**, *55*, 4203–4225. [[CrossRef](#)]
39. Singh, S. Sedimentation patterns of the Proterozoic Delhi Supergroup, northeastern Rajasthan, India, and their tectonic implications. *Sediment. Geol.* **1988**, *58*, 79–94. [[CrossRef](#)]
40. Azam, M.S.; Khan, M.S.; Raza, M. Petrogenetic study of Mesoproterozoic volcanic rocks of North Delhi fold belt, NW Indian shield: Implications for mantle conditions during Proterozoic. *Chin. J. Geochem.* **2014**, *34*, 93–114. [[CrossRef](#)]

41. Kaur, P.; Zeh, A.; Chaudhri, N. U–Pb age and Hf isotope record of detrital zircon grains from the North Delhi Supergroup, NW India: Implications for provenance and stratigraphic correlations. *Int. J. Earth Sci.* **2019**, *108*, 2683–2697. [[CrossRef](#)]
42. Das Gupta, S.P. The structural history of the Khetri Copper Belt, Jhunjhunu and Sikar districts, Rajasthan. *Mem. Geol. Surv. India* **1968**, *98*, 170.
43. Das, A.R. Geometry of the superposed deformation in the Delhi Supergroup rocks, North of Jaipur, Rajasthan. In *Precambrian of the Aravalli Mountain, Rajasthan, India*; Roy, A.B., Ed.; Memoir Geological Society of India: Bangalore, India, 1988; Volume 7, pp. 257–266.
44. Naha, K.; Mukhopadhyay, D.K.; Mohanty, R. Structural evolution of the rocks of the Delhi Group around Khetri, north-eastern Rajasthan. In *Precambrian of the Aravalli Mountain, Rajasthan, India*; Roy, A.B., Ed.; Memoir Geological Society of India: Bangalore, India, 1988; Volume 7, pp. 207–245.
45. Gangopadhyay, P.K.; Sen, R. Trend of regional metamorphism: An example from “Delhi System” of rocks occurring around Bairawas, north-eastern Rajasthan. *India. Geol. Rundsch* **1972**, *61*, 270–281. [[CrossRef](#)]
46. Lal, R.K.; Ackermann, D. Phase petrology and polyphase andalusite-sillimanite type regional metamorphism in pelitic schist of the area around Akwali, Khetri Copper Belt, Rajasthan, India. *Neues Jahrb. Mineral. Abhandl.* **1981**, *141*, 161–185.
47. Kaur, P.; Zeh, A.; Okrusch, M.; Chaudhri, N.; Gerdes, A.; Brätz, H. Separating regional metamorphic and metasomatic assemblages and events in the northern Khetri complex, NW India: Evidence from mineralogy, whole-rock geochemistry and U–Pb monazite chronology. *J. Asian Earth Sci.* **2016**, *129*, 117–141. [[CrossRef](#)]
48. Baidya, A.S.; Paul, J.; Pal, D.C.; Upadhyay, D. Mode of occurrence and geochemistry of amphiboles in the Kolihan–Chandmari copper deposits, Rajasthan, India: Insight into the ore-forming process. *Ore Geol. Rev.* **2017**, *80*, 1092–1110. [[CrossRef](#)]
49. Li, X.C.; Zhou, M.F.; Williams-Jones, A.E.; Yang, Y.H.; Gao, J.F. Timing and genesis of CU–(Au) mineralization in the Khetri Copper Belt, north western India: Constraints from in situ U–Pb ages and Sm–Nd isotopes of monazite–(Ce). *Miner. Dep.* **2019**, *54*, 553–569. [[CrossRef](#)]
50. Mehdi, M.; Kumar, S.; Pant, N.C. Low grade metamorphism in the Lalsot-Bayana sub-basin of the North Delhi Fold Belt and its tectonic implication. *J. Geol. Soc. India* **2015**, *85*, 397–410. [[CrossRef](#)]
51. Boopathi, D. Investigation for copper and associated precious metals, Mundiyawas-Khera area, Alwar district, Rajasthan. *Geol. Surv. India Rep. FS* **2010**, 2008–2009, Unpublished.
52. Khan, I. Metallogenetic Significance and Exploration Strategies of Copper-Gold Mineralization near Mundiyawas-Khera Area, Alwar Basin, Rajasthan, Western India. Ph.D. Thesis, Indian Institute of Technology (Indian School of Mines), Dhanbad, India, 2021. Unpublished.
53. Satyanarayanan, M.; Balaram, V.; Sawant, S.S.; Subramanyam, K.S.V.; Krishna, G.V.; Dasaram, B.; Manikyamba, C. Rapid determination of REEs, PGEs, and other trace elements in geological and environmental materials by high resolution inductively coupled plasma mass spectrometry. *At. Spectrosc.* **2018**, *39*, 1–15. [[CrossRef](#)]
54. Piercy, S.J.; Peter, J.M.; Mortensen, J.K.; Paradis, S.; Murphy, D.C.; Tucker, T.L. Petrology and U–Pb Geochronology of Footwall Porphyritic Rhyolites from the Wolverine Volcanogenic Massive Sulfide Deposit, Yukon, Canada: Implications for the Genesis of Massive Sulfide Deposits in Continental Margin Environments. *Econ. Geol.* **2008**, *103*, 5–33. [[CrossRef](#)]
55. Lentz, D.R. Petrogenetic evolution of felsic volcanic sequences associated with Phanerozoic volcanic-hosted massive sulphide systems: The role of extensional geodynamics. *Ore Geol. Rev.* **1998**, *12*, 289–327. [[CrossRef](#)]
56. Le Bas, M.J.; Le Maitre, R.W.; Streckeisen, A.; Zannettin, B. A chemical classification of volcanic rocks based on the total alkali-silica diagram. *J. Petrol.* **1986**, *27*, 745–750. [[CrossRef](#)]
57. Winchester, J.A.; Floyd, P.A. Geochemical discrimination of different magma series and their differentiation products using immobile elements. *Chem. Geol.* **1977**, *20*, 325–343. [[CrossRef](#)]
58. Ross, P.S.; Bédard, J.H. Magmatic affinity of modern and ancient subalkaline volcanic rocks determined from trace-element discriminant diagrams. *Can. J. Earth Sci.* **2009**, *46*, 823–839. [[CrossRef](#)]
59. Shand, S.J. *The Eruptive Rocks*, 2nd ed.; John Wiley and Sons: New York, NY, USA, 1943; 444p.
60. Piercy, S.J. The setting, style, and role of magmatism in the formation of volcanogenic massive sulfide deposits. *Miner. Depos.* **2011**, *46*, 449–471. [[CrossRef](#)]
61. Whalen, J.B.; Struik, L.C.; Hrudey, M.G. Bedrock geology of the Endako map area, central British Columbia. *Curr. Res.* **1998**, 113–123.
62. Large, R.R.; Gemmell, J.B.; Paulick, H.; Huston, D.L. The alteration box plot: A simple approach to understanding the relationship between alteration mineralogy and lithogeochemistry associated with volcanic-hosted massive sulfide deposits. *Econ. Geol.* **2001**, *96*, 957–971. [[CrossRef](#)]
63. Taylor Jr, H.P.; Frechen, J.; Degens, E.T. Oxygen and carbon isotope studies of carbonatites from the Laacher See District, West Germany and the Alnö District, Sweden. *Geochim. Cosmochim. Acta* **1967**, *31*, 407–430. [[CrossRef](#)]
64. Veizer, J.; Hoefs, J. The nature of O<sub>18</sub>/O<sub>16</sub> and C<sub>13</sub>/C<sub>12</sub> secular trends in sedimentary carbonate rocks. *Geochim. Cosmochim. Acta* **1976**, *40*, 1387–1395. [[CrossRef](#)]
65. Demény, A.; Ahijado, A.; Casillas, R.; Vennemann, T. Crustal contamination and fluid/rock interaction in the carbonatites of Fuerteventura (Canary Islands, Spain): A C, O, H isotope study. *Lithos* **1998**, *44*, 101–115. [[CrossRef](#)]
66. Hoefs, J. *Stable Isotope Geochemistry*; Springer: Berlin/Heidelberg, Germany, 2009; Volume 285.

67. Zhang, W.; Deng, X.; Peng, L.; Zhang, Y.; Xu, D.; Liu, H.; Jin, X.; Sun, J.; Lai, C. Rare earth elements and car-bon-oxygen isotopes of calcite from the Tongjiachong Cu deposit, South China: Implications for fluid source and mineral precipitation. *Ore Geol. Rev.* **2020**, *116*, 103236. [[CrossRef](#)]
68. Du, L.J.; Li, B.; Huang, Z.L.; Zhou, J.X.; Zou, G.F.; Yan, Z.F. Carbon-oxygen isotopic geochemistry of the Yangla Cu skarn deposit, SW China: Implications for the source and evolution of hydrothermal fluids. *Ore Geol. Rev.* **2017**, *88*, 809–821. [[CrossRef](#)]
69. Huston, D.L. Stable isotopes and the genesis of volcanic-hosted massive sulfide deposits: A review, in volcanic-ic-associated massive sulfide deposits: Processes and examples in modern and ancient settings. *Rev. Econ. Geol.* **1999**, *8*, 157–179.
70. Holland, H.D. The solubility and occurrence of non-ore minerals. *Geochem. Hydrothermal Ore Depos.* **1979**, *461*–508.
71. Zheng, Y.F. The effect of Rayleigh degassing of magma on sulphur isotope composition: A quantitative evaluation. *Terra Nova* **1990**, *2*, 74–78. [[CrossRef](#)]
72. Matsuhisa, Y.; Morishita, Y.; Sato, T. Oxygen and carbon isotope variations in gold-bearing hydrothermal veins in the Kushikino mining area, southern Kyushu, Japan. *Econ. Geol.* **1985**, *80*, 283–293. [[CrossRef](#)]
73. Huston, D.L. Stable Isotopes and Their Significance for Understanding the Genesis of Volcanic-Hosted Massive Sulfide Deposits: A Review. In *Volcanic Associated Massive Sulfide Deposits: Processes and Examples in Modern and Ancient Settings*; Barrie, C.T., Hannington, M.D., Eds.; Society of Economic Geologists: Littleton, CO, USA, 1997. [[CrossRef](#)]
74. Hajsadeghi, S.; Mirmohammadi, M.; Asghari, O.; Meshkani, S.A. Geology and mineralization at the copper-rich volcanogenic massive sulfide deposit in Nohkouhi, Posht-e-Badam block, Central Iran. *Ore Geol. Rev.* **2018**, *92*, 379–396. [[CrossRef](#)]
75. Lesher, C.M.; Goodwin, A.M.; Campbell, I.; Gorton, M.P. Trace-element geochemistry of ore-associated and barren, felsic metavolcanic rocks in the Superior Province, Canada. *Can. J. Earth Sci.* **1986**, *23*, 222–237. [[CrossRef](#)]
76. Hart, T.R.; Gibson, H.L.; Lesher, C.M. Trace element geochemistry and petrogenesis of felsic volcanic rocks associated with volcanogenic massive Cu-Zn-Pb sulfide deposits. *Econ. Geol.* **2004**, *99*, 1003–1013. [[CrossRef](#)]
77. Piercy, S.J.; Paradis, S.; Murphy, D.C.; Mortensen, J.K. Geochemistry and Paleotectonic Setting of Felsic Volcanic Rocks in the Finlayson Lake Volcanic-Hosted Massive Sulfide District, Yukon, Canada. *Econ. Geol.* **2001**, *96*, 1877–1905. [[CrossRef](#)]
78. Pearce, J.A.; Harris, N.B.W.; Tindle, A.G. Trace Element Discrimination Diagrams for the Tectonic Interpretation of Granitic Rocks. *J. Pet.* **1984**, *25*, 956–983. [[CrossRef](#)]
79. Pearce, J.A. Geochemical fingerprinting of oceanic basalts with applications to ophiolite classification and the search for Archean oceanic crust. *Lithos* **2008**, *100*, 14–48. [[CrossRef](#)]
80. Eby, G.N. Chemical subdivision of the A-type granitoids: Petrogenetic and tectonic implications. *Geology* **1992**, *20*, 641–644. [[CrossRef](#)]
81. McDonough, W.F.; Sun, S.S. The composition of the Earth. *Chem. Geol.* **1995**, *120*, 223–253. [[CrossRef](#)]
82. Barrett, T.J.; MacLean, W.H. Volcanic sequences, lithogeochemistry and hydrothermal alteration in some bimodal volcanic-associated massive sulfide systems. In *Volcanic Associated Massive Sulfide Deposits: Processes and Examples in Modern and Ancient Settings*; Barrie, C.T., Hannington, M.D., Eds.; Society of Economic Geologists: Shaffer Parkway Littleton, CO, USA, 1999; Volume 8, pp. 101–131.
83. Piercy, S.J. An overview of the use of petrochemistry in regional exploration for volcanogenic massive sulfide (VMS) deposits. In Proceedings of the Exploration 07: Fifth Decennial International Conference on Mineral Exploration, Toronto, ON, Canada, 9–12 September 2007; Milkereit, B., Ed.; pp. 223–246.
84. Boynton, W.V. Geochemistry of Rare Earth Elements: Meteorite Studies. In *Rare Earth Element Geochemistry*; Henderson, P., Ed.; Elsevier: New York, NY, USA, 1984; pp. 63–114.
85. Lottermoser, B. Rare earth element study of exhalites within the Willyama supergroup, Broken Hill Block, Australia. *Miner. Deposita* **1989**, *24*, 92–99. [[CrossRef](#)]
86. Sun, S.S.; McDonough, W.F. Chemical and isotopic systematics of oceanic basalts: Implications for mantle composition and processes. *Geol. Soc. London UK Spec. Publ.* **1989**, *42*, 313–345. [[CrossRef](#)]
87. Solomon, M.; Wolf, K. “Volcanic” massive sulphide deposits and their host rocks—A review and an explanation. *Handb. Stratif. Ore Depos.* **1976**, *6*, 21–54.
88. Eldridge, C.S.; Barton, P.B.; Ohmoto, H. Mineral textures and their bearing on the formation of the Kuroko deposits. In *The Kuroko and Related Volcanogenic Massive Sulphide Deposits*; Ohmoto, H., Skinner, B.J., Eds.; Society of Economic Geologists: Shaffer Parkway Littleton, CO, USA, 1983; Volume 5, pp. 241–281.
89. Lydon, J.W. ‘Volcanogenic massive sulphide deposits’ Part 1. A descriptive model; Geoscience Canada Reprint Series 3. *Ore Depos. Models-8* **1988**, *11*, 145–152.
90. Large, R.R. Australian volcanic-hosted massive sulphide deposits, features, styles, and genetic models. *Econ. Geol.* **1992**, *87*, 471–510. [[CrossRef](#)]
91. Ohmoto, H. Formation of volcanogenic massive sulfide deposits: The Kuroko perspective. *Ore Geol. Rev.* **1996**, *10*, 135–177. [[CrossRef](#)]
92. Sánchez-España, J.; Velasco, F.; Boyce, A.J.; Fallick, A.E. Source and evolution of ore-forming hydrothermal fluids in the northern Iberian Pyrite Belt massive sulphide deposits (SW Spain): Evidence from fluid inclusions and stable isotopes. *Miner. Deposita* **2002**, *38*, 519–537. [[CrossRef](#)]
93. Relvas, J.M.R.S. Geology and Metallogenesis at the Neves Corvo Deposit, Portugal. Ph.D. Thesis, University of Lisbon, Lisbon, Portugal, 2000.

94. Rao, V.V.; Prasad, B.R.; Reddy, P.R.; Tewari, H.C. Evolution of Proterozoic Aravalli Delhi fold belt in the north-western Indian shield from seismic studies. *Tectonophysics* **2000**, *327*, 109–130.
95. Raza, M.; Khan, M.; Azam, M. Plate-plume-accretion tectonics in Proterozoic terrain of northeastern Rajasthan, India: Evidence from mafic volcanic rocks of north Delhi fold belt. *Island Arc.* **2007**, *16*, 536–552. [CrossRef]
96. Ravikant, V.; Golani, P.R. Rb-Sr direct dating of pyrite from the Pipela VMS Zn-Cu prospect, Rajasthan, NW India. *J. Geol. Soc. India* **2011**, *77*, 149–159. [CrossRef]
97. Praveen, M.; Nambiar, C.; Huston, D.L. Geochemistry and petrogenesis of Paleoproterozoic rhyolite-hosted zinc-rich metamorphosed volcanogenic massive sulfide deposits in the eastern Betul Belt, central India. *Ore Geol. Rev.* **2020**, *131*, 103918. [CrossRef]
98. *Geology and Mineral Resources of India: Miscellaneous Publication No. 30, Part-XXII*; Director General, Geological Survey of India: Kolkata, India; ISSN 0579-4706.
99. Shanks, W.C., III. Hydrothermal alteration in volcanogenic massive sulfide occurrence model. *United States Geol. Surv. Sci. Investig. Rep.* **2010**, *5070*, 12.
100. Slack, J.F.; Causey, J.D.; Eppinger, R.G.; Gray, J.E.; Johnson, C.A.; Lund, K.I.; Schulz, K.J. Co-Cu-Au Deposits in Metasedimentary Rocks—A Preliminary Report: U.S. Geological Survey Open-File Report 2010–2012. 2010; p. 13. Available online: <http://pubs.usgs.gov/of/2010/1212/> (accessed on 15 March 2022).
101. Corbett, K.D. New mapping and interpretations of the Mount Lyell mining district, Tasmania: A large hybrid Cu-Au system with an exhalative Pb-Zn top. *Econ. Geol.* **2001**, *96*, 1089–1122. [CrossRef]
102. Huston, D.L.; Kamprad, J. Zonation of alteration facies at western Tharsis: Implications for the genesis of Cu-Au deposits, Mount Lyell field, western Tasmania. *Econ. Geol.* **2001**, *96*, 1123–1132. [CrossRef]
103. Kerr, D.J.; Gibson, H.L. A comparison of the Horne volcanogenic massive sulfide deposit and intracauldron de-positos of the Mine Sequence, Noranda, Quebec. *Econ. Geol.* **1993**, *88*, 1419–1442. [CrossRef]
104. Praveen, M.N. Geochemistry and Petrogenesis of Rhyolites Hosting VMS Mineralisation in the Eastern Betul Belt, Central India. Ph.D. Thesis, Department of Marine Geology and Geophysics, School of Marine Sciences, Cochin University of Science and Technology, Cochin, India, 2016.